Meccanica (2018) 53:2503–2523
https://doi.org/10.1007/s11012-018-0836-0

A phenomenological description of shape memory alloy transformation induced plasticity

Sergio de A. Oliveira · Vanderson M. Dornelas · Marcelo A. Savi · Pedro Manuel C. L. Pacheco · Alberto Paiva

Received: 24 August 2017 / Accepted: 16 February 2018 / Published online: 27 February 2018

Abstract Transformation induced plasticity is defined as the plastic flow arising from solid state phase transformation processes involving volume and/or shape changes without overlapping the yield surface. This phenomenon occurs in shape memory alloys (SMAs) having significant influence over their macroscopic thermomechanical behavior. This contribution presents a macroscopic three-dimensional constitutive model to describe the thermomechanical behavior of SMAs including classical and transformation induced plasticity. Comparisons between numerical and experimental results attest the model capability to capture plastic phenomena. Both uniaxial and multiaxial simulations are carried out.

Keywords Shape memory alloys · Classical plasticity · Transformation induced plasticity · Constitutive model · Numerical simulations

V. M. Dornelas · M. A. Savi (✉)
COPPE – Department of Mechanical Engineering, Center for Nonlinear Mechanics, Universidade Federal do Rio de Janeiro, P.O. Box 68.503, 21.941.972, Rio de Janeiro, RJ, Brazil
e-mail: vm.dornelas@mecanica.coppe.ufrj.br

M. A. Savi
e-mail: savi@mecanica.ufrj.br

S. A. Oliveira · P. M. C. L. Pacheco
Department of Mechanical Engineering, CEFET/RJ – Centro Federal de Educação Tecnológica Celso Suckow da Fonseca, 20.271.110, Rio de Janeiro, RJ, Brazil
e-mail: amserol@yahoo.com.br

P. M. C. L. Pacheco
e-mail: pedro.pacheco@cefet-rj.br

A. Paiva
Volta Redonda School of Engineering - Department of Mechanical Engineering, Universidade Federal Fluminense, 27.255.250, Volta Redonda, RJ, Brazil
e-mail: albertopaiva@id.uff.br

1 Introduction

Shape memory alloys (SMAs) belong to the class of smart materials that have complex thermomechanical behavior related to different physical phenomena. Basically, the coupling between different physical fields establishes the remarkable properties of SMAs. Among the main behaviors, shape memory effect should be highlighted, where the specimen can recover its original geometry by the imposition of a proper thermomechanical loading process. Pseudoelasticity or superelasticity, two-way shape memory effect, phase transformation due to temperature variation, internal subloops due to incomplete phase transformation, and tension–compression asymmetry are other important behaviors identified on SMAs [17, 25].

Plastic behavior of SMAs can be described by two different mechanisms: classical plasticity and transformation induced plasticity (TRIP). The classical

plasticity arises from applied stress or temperature variation when yield surface is reached. On the other hand, TRIP results from internal stresses arising either from the volume change associated with the transformation or from the accompanying shape change without reaching the yield surface of the weaker phase involved [7, 8, 12, 13, 20, 23, 36].

TRIP phenomenon is usually associated with two distinct physical mechanisms, which have been proposed by Greenwood and Johnson [14] and Magee [22]. The Greenwood-Johnson effect is admitted to be due to an accommodation process of the microplasticity associated with a volume change. The Magee effect, on the other hand, is due to an orientation effect that arises from a shear internal stress state, which favors the thermodynamically preferred orientation direction for martensite formation in the presence of an external stress field, involving shape change.

According to Greenwood and Johnson [14], TRIP is due to the compactness difference between parent (austenite) and product (martensite) phase lattice structures. During martensitic transformation, this difference results in a volume change, producing a microscopic internal stress state, responsible for microscopic plasticity in the weaker phase (with the lower yielding stress). Without external applied stress, the average of these internal stresses generally vanishes and, from macroscopic point of view, only global variation of the volume is observed. In order to understand the Magee effect, consider the martensitic formation process on cooling. During its nucleation, martensite develops plates that grow and generate large amounts of shear stress in the parent austenitic matrix [7]. When external load is not applied, the plate orientation is generally random, which makes the macroscopic resultant of the microscopic internal stresses average out null. An external applied load triggers an alignment of these martensitic plates with the loading stress direction. This external load is responsible for an internal stress state increase that no more will macroscopically average out null [34].

Many efforts have been done towards TRIP modeling [3, 7, 10, 19, 20, 23, 36–35, 44]. The majority of these models focuses on micro scale features of the TRIP. Moreover, some of them discard the Magee effect under some reasonable considerations for particular studies.

Concerning TRIP effect on SMAs, it should be pointed out that SMAs present reversible phase transformations that are different from common steels. Hence, after a cyclic loading, SMA presents a TRIP strain generated by a competition between the ones generated during forward and reverse transformations [43]. Some studies related to cyclic loading responses of SMAs should be highlighted, such as: Tanaka et al. [37], Piecyska et al. [28], Lagoudas et al. [16], Auricchio et al. [1], Kang et al. [15] and Yu et al. [41]. The main characteristic observed in the stress–strain curves during cyclic loading process is the reduction of the phase transformation stress and the increase of the residual permanent strain, which characterizes the TRIP effect [1]. This feature establishes a training process in order to stabilize stress–strain curves before the use of SMA for applications. Paradis et al. [27] simulated the degradation behavior of NiTi shape memory alloy observed during uniaxial cyclic loading. Freed and Aboudi [9] investigated thermomechanical coupled SMA model for composites undergoing TRIP effect. Entchev and Lagoudas [6] and Lagoudas and Entchev [18] discussed the modeling of the TRIP effect for porous SMAs. Zaki and Mounmi [42] discussed a three-dimensional model to describe SMA behavior subjected to cyclic loadings. Cissé et al. [4], Sakhaei and Lim [29] and Chemisky et al. [2] are other research efforts to treat SMA subjected to cyclic loading process.

Yu et al. [40, 39] proposed a one-dimensional constitutive model by considering two different inelastic deformation mechanisms: phase transformation and TRIP. The proposed model employed evolution rules associated with the dislocation slipping in the austenite phase near the austenite–martensite interfaces. In addition, anisotropic cyclic deformation of superelastic NiTi was of concern.

This paper presents a three-dimensional constitutive model with internal constraints, which accounts for both classical and transformation induced plasticity. The proposed model is an extension of the one presented by Oliveira et al. [24] that is inspired on the one-dimensional model presented in Paiva et al. [26]. The goal of this work is to describe the macroscopic manifestation of the TRIP phenomenon on SMAs, exploring its influence on cyclic loadings. Classical plasticity is also incorporated on the proposed

constitutive model. Comparisons between numerical and experimental results are used to show the model ability to capture the general thermomechanical behavior of SMAs, including TRIP and classical plasticity. Numerical simulations are carried out considering both uniaxial and multiaxial tests in order to evaluate saturation mechanisms during cyclic loadings.

2 Constitutive model

The three-dimensional description of SMA thermomechanical behavior is based on the previous model presented in Oliveira et al. [24]. This model is developed within the framework of continuum mechanics and generalized standard materials approach [21], being inspired on the one-dimensional model proposed by Paiva et al. [26]. Under this assumption, the thermomechanical behavior can be described by the Helmholtz free energy density, Ψ, and the pseudo-potential of dissipation, Φ. This approach assures that the second law of thermodynamics is automatically satisfied, avoiding inconsistent behaviors.

2.1 Free energy density

The constitutive model adopts four macroscopic phases: austenite (A), twinned martensite (M), which is stable in the absence of a stress field, and two other variants associated with detwinned martensite, M^+ and M^-. The use of this limit number of martensitic variants is possible due to the definition of an equivalent strain field, Γ, which induces phase transformations. This definition is based on experimental observations that show that both volumetric and deviatoric effects induce phase transformations with the same qualitative behavior. Under this assumption, the equivalent field Γ may be interpreted as a phase transformation inductor that defines which kind of martensitic variant is induced, being expressed by the following equation where summation convention is evoked.

$$\Gamma = \frac{1}{3}\varepsilon^e_{kk} + \frac{2}{3}\sqrt{3J^e_2}\,\mathrm{sign}\left(\varepsilon^e_{kk}\right) \tag{1}$$

Note that this strain field has volumetric and deviatoric terms that are respectively given by:

$$\varepsilon^e_{kk} = \varepsilon^e_{11} + \varepsilon^e_{22} + \varepsilon^e_{33} \tag{2}$$

$$J^e_2 = \frac{1}{6}\hat{\varepsilon}^e_{ij}\hat{\varepsilon}^e_{ij} = \frac{1}{6}\Big\{\left(\varepsilon^e_{11}-\varepsilon^e_{22}\right)^2+\left(\varepsilon^e_{22}-\varepsilon^e_{33}\right)^2 + \left(\varepsilon^e_{33}-\varepsilon^e_{11}\right)^2+6\Big[\left(\varepsilon^e_{12}\right)^2+\left(\varepsilon^e_{13}\right)^2+\left(\varepsilon^e_{23}\right)^2\Big]\Big\} \tag{3}$$

where the deviatoric elastic strain is given by

$$\hat{\varepsilon}^e_{ij} = \varepsilon^e_{ij} - \frac{1}{3}\varepsilon^e_{kk}\delta_{ij} \tag{4}$$

and

$$\mathrm{sign}\left(\varepsilon^e_{kk}\right) = \begin{cases} +1, & \text{if } \varepsilon^e_{kk} \geq 0 \\ -1, & \text{if } \varepsilon^e_{kk} < 0 \end{cases} \tag{5}$$

TRIP effect is described by introducing new internal variables related to saturation effect during the cyclic loadings. Helmholtz free energy density is defined by considering different expressions for each one of the macroscopic phases, assuming that they are functions of elastic strain ε^e_{ij}, temperature, T, isotropic hardening variable, ϑ, and kinematic hardening tensor, ς_{ij}. Basically, the same structure proposed by Oliveira et al. [24] is adopted resulting in the following energy density functions:

$$\begin{aligned}
M^+ &: \rho\Psi^+\left(\varepsilon^e_{ij}, T, \vartheta, \varsigma_{ij}\right) \\
&= \frac{1}{2}\left(\lambda^M\varepsilon^e_{kk}\varepsilon^e_{pp} + 2\mu^M\varepsilon^e_{ij}\varepsilon^e_{ij}\right) - \alpha\Gamma - \Lambda^M \\
&\quad - \Omega^M_{ij}(T-T_0)\varepsilon^e_{ij} + \frac{1}{2}K^M\vartheta^2 + \frac{1}{2H^M}\varsigma_{ij}\varsigma_{ij} \\
M^- &: \rho\Psi^-\left(\varepsilon^e_{ij}, T, \vartheta, \varsigma_{ij}\right) \\
&= \frac{1}{2}\left(\lambda^M\varepsilon^e_{kk}\varepsilon^e_{pp} + 2\mu^M\varepsilon^e_{ij}\varepsilon^e_{ij}\right) + \alpha\Gamma - \Lambda^M \\
&\quad - \Omega^M_{ij}(T-T_0)\varepsilon^e_{ij} + \frac{1}{2}K^M\vartheta^2 + \frac{1}{2H^M}\varsigma_{ij}\varsigma_{ij} \\
A &: \rho\Psi^A\left(\varepsilon^e_{ij}, T, \vartheta, \varsigma_{ij}\right) \\
&= \frac{1}{2}\left(\lambda^A\varepsilon^e_{kk}\varepsilon^e_{pp} + 2\mu^A\varepsilon^e_{ij}\varepsilon^e_{ij}\right) - \Lambda^A - \Omega^A_{ij}(T-T_0)\varepsilon^e_{ij} \\
&\quad + \frac{1}{2}K^A\vartheta^2 + \frac{1}{2H^A}\varsigma_{ij}\varsigma_{ij} \\
M &: \rho\Psi^M\left(\varepsilon^e_{ij}, T, \vartheta, \varsigma_{ij}\right) \\
&= \frac{1}{2}\left(\lambda^M\varepsilon^e_{kk}\varepsilon^e_{pp} + 2\mu^M\varepsilon^e_{ij}\varepsilon^e_{ij}\right) + \Lambda^M - \Omega^M_{ij}(T-T_0)\varepsilon^e_{ij} \\
&\quad + \frac{1}{2}K^M\vartheta^2 + \frac{1}{2H^M}\varsigma_{ij}\varsigma_{ij}
\end{aligned} \tag{6}$$

In the previous equations, subscript A and M are related to austenite and martensitic phases, respectively; λ and μ are the Lamé coefficients; α is a parameter that control the height of the stress–strain hysteresis loop; Λ^M and Λ^A are functions of temperature that define the phase transformation stress value; Ω_{ij} is a tensor related to the thermal expansion coefficients; T_0 is a reference temperature in a stress-free state; K it is the plastic modulus; H is the kinematical hardening modulus; and finally, ρ is the material density.

The free energy density of the mixture is defined by setting the volume fraction of martensitic variants, β^+ and β^-, associated with detwinned martensites (M^+ and M^-, respectively) and β^A that stands for the austenite (A). The fourth phase is associated with twinned martensite (M) and its volume fraction is β^M. Since $\beta^M = 1 - \beta^+ - \beta^- - \beta^A$, it is possible to define a free energy density in terms of three volume fractions. Moreover, it is assumed new internal variables specifically related to the TRIP phenomenon: $\xi^+, \xi^-$and ξ^A. Thus, the total free energy is given by:

$$\begin{aligned}&\rho\Psi\left(\varepsilon^e_{ij}, T, \vartheta, \varsigma_{ij}, \beta^+, \beta^-, \beta^A, \xi^+, \xi^-, \xi^A\right)\\ &= \rho[\beta^+\left(\Psi^+ - \Psi^M\right) + \beta^-\left(\Psi^- - \Psi^M\right)\\ &\quad + \beta^A\left(\Psi^A - \Psi^M\right) + \Psi^M] + I_\pi\left(\beta^+, \beta^-, \beta^A\right)\end{aligned} \tag{7}$$

where $I_\pi\left(\beta^+, \beta^-, \beta^A\right)$ is the indicator function associated with the convex π representing phase coexistence.

$$\pi = \left\{\beta^m \in \Re \middle| 0 \le \beta^m \le 1 (m = +, -, A); \beta^+ + \beta^- + \beta^A \le 1\right\} \tag{8}$$

Substituting the individual Helmholtz free energy density into Eq. (7), the free energy density of the mixture assumes the following form:

$$\begin{aligned}&\rho\Psi\left(\varepsilon^e_{ij}, T, \vartheta, \varsigma_{ij}, \beta^+, \beta^-, \beta^A, \xi^+, \xi^-, \xi^A\right)\\ &= \Gamma\alpha\left(\beta^- - \beta^+\right) - \Lambda\left(\beta^+ + \beta^-\right)\\ &\quad + \left[\frac{1}{2}\left(\lambda^A - \lambda^M\right)\varepsilon^e_{kk}\varepsilon^e_{pp} + \left(\mu^A - \mu^M\right)\varepsilon^e_{ij}\varepsilon^e_{ij}\right.\\ &\quad - \left(\Omega^A_{ij} - \Omega^M_{ij}\right)(T - T_0)\varepsilon^e_{ij} - \Lambda^{\aleph}\\ &\quad \left.+\frac{1}{2}\left(K^A - K^M\right)\vartheta^2 + \left(\frac{1}{2H^A} - \frac{1}{2H^M}\right)\varsigma_{ij}\varsigma_{ij}\right]\beta^A\\ &\quad + \left[\frac{1}{2}\lambda^M\varepsilon^e_{kk}\varepsilon^e_{pp} + \mu^M\varepsilon^e_{ij}\varepsilon^e_{ij}\right]\\ &\quad - \Omega^M_{ij}(T - T_0)\varepsilon^e_{ij} + \Lambda^{\aleph} + \frac{1}{2}K^M\vartheta^2 + \frac{1}{2H^M}\varsigma_{ij}\varsigma_{ij}\\ &\quad + I_\pi\left(\beta^+, \beta^-, \beta^A\right)\end{aligned} \tag{9}$$

An additive decomposition is assumed considering that the elastic strain is given by:

$$\varepsilon^e_{ij} = \varepsilon_{ij} - \varepsilon^t_{ij} - \varepsilon^p_{ij} - \varepsilon^{trip}_{ij} \tag{10}$$

where ε_{ij} is the total strain, ε^p_{ij} is the plastic strain and ε^{trip}_{ij} is the TRIP strain. The phase transformation strain, ε^t_{ij}, is written as follows:

$$\varepsilon^t_{ij} = \alpha^h_{ijkl} r_{kl}\left(\beta^+ - \beta^-\right)\mathrm{sign}\left(\varepsilon^e_{kk}\right) \tag{11}$$

where α^h_{ijkl} is a fourth-order tensor related to phase transformations that considers a form that is similar to the classical isotropic elastic tensor. Due to symmetries, it can be expressed as a matrix, considering different parameters for normal, α^h_N, and shear, α^h_S, behaviors,

$$\alpha^h_{ijkl} \equiv \begin{bmatrix} \alpha^h_N & \alpha^h_N - \alpha^h_S & \alpha^h_N - \alpha^h_S & 0 & 0 & 0\\ \alpha^h_N - \alpha^h_S & \alpha^h_N & \alpha^h_N - \alpha^h_S & 0 & 0 & 0\\ \alpha^h_N - \alpha^h_S & \alpha^h_N - \alpha^h_S & \alpha^h_N & 0 & 0 & 0\\ 0 & 0 & 0 & \alpha^h_S & 0 & 0\\ 0 & 0 & 0 & 0 & \alpha^h_S & 0\\ 0 & 0 & 0 & 0 & 0 & \alpha^h_S \end{bmatrix} \tag{12}$$

The definition of transformation strain employs parameter r_{kl} that is a symmetric second-order tensor related to the loading history as follows:

$$r_{kl} = \begin{cases} +1, & \text{if } \sigma_{kl} > 0\\ 0, & \text{if } \sigma_{kl} = 0\\ -1, & \text{if } \sigma_{kl} < 0 \end{cases} \tag{13}$$

For situations where mechanical loadings are provided by multiaxial, non-simultaneous load history, tensor r_{kl} is evaluated as follows for the subsequent loadings (assuming stress driving cases):

$$r_{kl} = \frac{\sigma_{kl}}{\left|S_{kl}^{\max}\right|}, \quad \text{if } \beta^{+} \neq 0 \text{ or } \beta^{-} \neq 0 \tag{14}$$

where $S_{kl}^{\max}$ represents the maximum value of the mechanical loading that can be a stress or a strain. Besides, note that $\frac{S_{kl}^{\max}}{\left|S_{kl}^{\max}\right|} = 0$ if $S_{kl}^{\max} = 0$.

2.1.1 Thermodynamic forces

From the generalized standard materials approach, the thermodynamical forces associated with its respective state variable are defined as follows [5, 21]:

$$\begin{aligned}\sigma_{ij} &= \rho\frac{\partial \Psi}{\partial \varepsilon_{ij}^{e}} \\ &= \lambda\varepsilon_{kk}^{e}\delta_{ij} + 2\mu\varepsilon_{ij}^{e} + \alpha\omega_{ij}\left(\beta^{-} - \beta^{+}\right) - \Omega_{ij}(T - T_0)\end{aligned} \tag{15}$$

$$\begin{aligned}B^{+} &\in -\rho\partial_{\beta^{+}}(\Psi) \\ &= \alpha\Gamma + \Lambda + P^{+} - \alpha_{ijkl}^{h} r_{kl}\Omega_{ij}(T - T_0) - \kappa_{\pi}^{+}\end{aligned} \tag{16}$$

$$\begin{aligned}B^{-} &\in -\rho\partial_{\beta^{-}}(\Psi) \\ &= -\alpha\Gamma + \Lambda + P^{-} + \alpha_{ijkl}^{h} r_{kl}\Omega_{ij}(T - T_0) - \kappa_{\pi}^{-}\end{aligned} \tag{17}$$

$$\begin{aligned}B^{A} &\in -\rho\partial_{\beta^{A}}(\Psi) \\ &= \Lambda^{\aleph} + P^{A} + \varepsilon_{ij}^{e}\left(\Omega_{ij}^{A} - \Omega_{ij}^{M}\right)(T - T_0) \\ &\quad - \frac{1}{2}\left(K^{A} - K^{M}\right)\vartheta^{2} \\ &\quad - \left(\frac{1}{2H^{A}} - \frac{1}{2H^{M}}\right)\varsigma_{ij}\varsigma_{ij} - \kappa_{\pi}^{A}\end{aligned} \tag{18}$$

$$\begin{aligned}X_{ij} &= -\rho\frac{\partial \Psi}{\partial \varepsilon_{ij}^{p}} \\ &= \lambda\varepsilon_{kk}^{e}\delta_{ij} + 2\mu\varepsilon_{ij}^{e} + \alpha\omega_{ij}\left(\beta^{-} - \beta^{+}\right) - \Omega_{ij}(T - T_0)\end{aligned} \tag{19}$$

$$\begin{aligned}R_{ij} &= -\rho\frac{\partial \Psi}{\partial \varepsilon_{ij}^{trip}} \\ &= \lambda\varepsilon_{kk}^{e}\delta_{ij} + 2\mu\varepsilon_{ij}^{e} + \alpha\omega_{ij}\left(\beta^{-} - \beta^{+}\right) - \Omega_{ij}(T - T_0)\end{aligned} \tag{20}$$

$$Y \in -\rho\frac{\partial \Psi}{\partial \vartheta} = -K\vartheta \tag{21}$$

$$Z_{ij} \in -\rho\frac{\partial \Psi}{\partial \varsigma_{ij}} = -\frac{1}{H}\varsigma_{ij} \tag{22}$$

$$S^{+} \in -\rho\frac{\partial \Psi}{\partial \xi^{+}} \tag{23}$$

$$S^{-} \in -\rho\frac{\partial \Psi}{\partial \xi^{-}} \tag{24}$$

$$S^{A} \in -\rho\frac{\partial \Psi}{\partial \xi^{A}} \tag{25}$$

where the thermodynamic forces B^{+}, B^{-}, B^{A} are related to phase transformations, X_{ij}, Y and Z_{ij} refer to classical plasticity, while R_{ij}, S^{+}, S^{-} and S^{A} are associated with TRIP effect being responsible for changes of the parameter nominal values; σ_{ij} represents the stress tensor; δ_{ij} is the Kronecker delta; $\kappa_{\pi}\left(\beta^{+}, \beta^{-}, \beta^{A}\right)$ is related to the sub-differential with respect to volume fractions being associated with projections in the β-space.

$$\kappa_{\pi} = \left(\kappa_{\pi}^{+}, \kappa_{\pi}^{-}, \kappa_{\pi}^{A}\right) \in \partial I_{\pi}\left(\beta^{+}, \beta^{-}, \beta^{A}\right) \tag{26}$$

Moreover, auxiliary quantities are defined as follows,

$$\omega_{ij} = \frac{1}{3}\delta_{ij} + \left[\frac{3\varepsilon_{ij}^{e} - \varepsilon_{kk}^{e}\delta_{ij}}{3\sqrt{3J_2^{e}}}\right]\operatorname{sign}\left(\varepsilon_{kk}^{e}\right) \tag{27}$$

$$\begin{aligned}P^{+} = &+ \left(\lambda\varepsilon_{mm}^{e}\alpha_{ijkl}^{h} r_{kl}\delta_{ij} + 2\mu\varepsilon_{ij}^{e}\alpha_{ijkl}^{h} r_{kl}\right) \\ &+ \alpha\left(\beta^{-} - \beta^{+}\right)\left\{\frac{1}{3}\alpha_{ijkl}^{h} r_{kl}\delta_{ij} + \frac{2P^{\alpha}}{\sqrt{3J_2^{e}}}\operatorname{sign}\left(\varepsilon_{kk}^{e}\right)\right\}\end{aligned} \tag{28}$$

$$P^{-} = -\left(\lambda\varepsilon^{e}_{mm}\alpha^{h}_{ijkl}r_{kl}\delta_{ij} + 2\mu\varepsilon^{e}_{ij}\alpha^{h}_{ijkl}r_{kl}\right) - \alpha\left(\beta^{-}-\beta^{+}\right)\left\{\frac{1}{3}\alpha^{h}_{ijkl}r_{kl}\delta_{ij} + \frac{2P^{\alpha}}{\sqrt{3J^{e}_{2}}}\operatorname{sign}\left(\varepsilon^{e}_{kk}\right)\right\} \tag{29}$$

$$P^{A} = -\frac{1}{2}\left(\lambda^{A}\left(\varepsilon^{e}_{kk}\right)^{2}+2\mu^{A}\varepsilon^{e}_{ij}\varepsilon^{e}_{ij}\right) + \frac{1}{2}\left(\lambda^{M}\left(\varepsilon^{e}_{kk}\right)^{2}+2\mu^{M}\varepsilon^{e}_{ij}\varepsilon^{e}_{ij}\right) \tag{30}$$

$$P^{\alpha} = \frac{\alpha^{h}_{S}}{6}\left\{(r_{11}-r_{22})\left(\varepsilon^{e}_{11}-\varepsilon^{e}_{22}\right) + (r_{22}-r_{33})\left(\varepsilon^{e}_{22}-\varepsilon^{e}_{33}\right) + (r_{33}-r_{11})\left(\varepsilon^{e}_{33}-\varepsilon^{e}_{11}\right) + 6\left(r_{12}\varepsilon^{e}_{12}+r_{13}\varepsilon^{e}_{13}+r_{23}\varepsilon^{e}_{23}\right)\right\} \tag{31}$$

2.2 Pseudo-potential of dissipation

The thermomechanical behavior of SMAs is intrinsically dissipative and therefore, it is necessary to establish a pseudo-potential of dissipation that allows the description of dissipation processes. It is assumed that this potential may be split into mechanical, Φ^{M}, and thermal, Φ^{H}, parts:

$$\Phi = \Phi^{M}\left(\dot{\varepsilon}^{e}_{ij}, \dot{\varepsilon}^{trip}_{ij}, \dot{\varepsilon}^{p}_{ij}, \dot{\vartheta}, \dot{\varsigma}_{ij}, \dot{\beta}^{+}, \dot{\beta}^{-}, \dot{\beta}^{A}, \dot{\xi}^{+}, \dot{\xi}^{-}, \dot{\xi}^{A}\right) + \Phi^{H}(q) \tag{32}$$

The dual of the mechanical pseudo-potential is presented as a function of thermodynamical forces,

$$\begin{aligned}\bar{\Phi}^{M}&\left(B^{+}, B^{-}, B^{A}, X_{ij}, Y, Z_{ij}, R_{ij}, S^{+}, S^{-}, S^{A}\right)\\ &= \frac{1}{2\eta^{+}}\left(B^{+}+\eta^{I}Y+\eta^{K}_{ij}Z_{ij}\right)^{2}\\ &\quad+\frac{1}{2\eta^{-}}\left(B^{-}\eta^{I}Y+\eta^{K}_{ij}Z_{ij}\right)^{2}+\frac{1}{2\eta^{A}}\left(B^{A}-\eta^{I}Y-\eta^{K}_{ij}Z_{ij}\right)^{2}\\ &\quad+\left(R_{ij}\right)^{2}\left\{\left(M_{13}\beta^{+}+M_{31}\beta^{A}\right)\dot{\beta}^{+}+\left(M_{32}\beta^{-}+M_{23}\beta^{A}\right)\dot{\beta}^{-}\right.\\ &\quad\left.+\left[M_{43}\beta^{A}+M_{34}\left(1-\beta^{+}-\beta^{-}-\beta^{A}\right)\right]\dot{\beta}^{A}\right\}+\left|\dot{\beta}^{+}\right|S^{+}\\ &\quad+\left|\dot{\beta}^{-}\right|S^{-}+\left|\dot{\beta}^{A}\right|S^{A}+I_{f}\left(X_{ij}, Y, Z_{ij}, R_{ij}, S^{+}, S^{-}, S^{A}\right)\\ &\quad+I_{\bar{\chi}}\left(B^{+}, B^{-}, B^{A}\right)\end{aligned} \tag{33}$$

The complementary equations for the thermodynamic fluxes are written as follows.

$$\begin{aligned}\dot{\beta}^{+} \in \partial_{B^{+}}\left(\bar{\Phi}^{\mathrm{M}}\right) &= \frac{B^{+}}{\eta^{+}}+\frac{\eta^{I}}{\eta^{+}}Y+\frac{\eta^{K}_{ij}}{\eta^{+}}Z_{ij}+\kappa^{+}_{\bar{\chi}}\\ &= \frac{B^{+}}{\eta^{+}}-\frac{\eta^{I}}{\eta^{+}}K\vartheta-\frac{\eta^{K}_{ij}}{\eta^{+}}\frac{\varsigma_{ij}}{H}+\kappa^{+}_{\chi}\end{aligned} \tag{34}$$

$$\begin{aligned}\dot{\beta}^{-} \in \partial_{B^{-}}\left(\bar{\Phi}^{\mathrm{M}}\right) &= \frac{B^{-}}{\eta^{-}}+\frac{\eta^{I}}{\eta^{-}}Y+\frac{\eta^{K}_{ij}}{\eta^{-}}Z_{ij}+\kappa^{-}_{\bar{\chi}}\\ &= \frac{B^{-}}{\eta^{-}}-\frac{\eta^{I}}{\eta^{-}}K\vartheta-\frac{\eta^{K}_{ij}}{\eta^{-}}\frac{\varsigma_{ij}}{H}+\kappa^{-}_{\chi}\end{aligned} \tag{35}$$

$$\begin{aligned}\dot{\beta}^{A} \in \partial_{B^{A}}\left(\bar{\Phi}^{\mathrm{M}}\right) &= \frac{B^{A}}{\eta^{A}}+\frac{\eta^{I}}{\eta^{A}}Y+\frac{\eta^{K}_{ij}}{\eta^{A}}Z_{ij}+\kappa^{A}_{\bar{\chi}}\\ &= \frac{B^{A}}{\eta^{A}}-\frac{\eta^{I}}{\eta^{A}}K\vartheta-\frac{\eta^{K}_{ij}}{\eta^{A}}\frac{\varsigma_{ij}}{H}+\kappa^{A}_{\chi}\end{aligned} \tag{36}$$

$$\dot{\varepsilon}^{p}_{ij} \in \partial_{X_{ij}}\left(\bar{\Phi}^{\mathrm{M}}\right) = \gamma\frac{\hat{\sigma}_{ij}-\varsigma_{ij}}{\|\hat{\sigma}_{ij}-\varsigma_{ij}\|} \tag{37}$$

$$\begin{aligned}\dot{\vartheta} \in \partial_{Y}\left(\bar{\Phi}^{\mathrm{M}}\right) &= \sqrt{\frac{2}{3}}\gamma+\eta^{I}\left(\dot{\beta}^{+}+\dot{\beta}^{-}+\dot{\beta}^{A}\right)\\ &= \sqrt{\frac{2}{3}}\left|\dot{\varepsilon}^{p}_{ij}\right|+\eta^{I}\left(\dot{\beta}^{+}+\dot{\beta}^{-}+\dot{\beta}^{A}\right)\end{aligned} \tag{38}$$

$$\begin{aligned}\dot{\varsigma}_{ij} \in \partial_{Z_{ij}}\left(\bar{\Phi}^{\mathrm{M}}\right) &= \frac{2}{3}\gamma H\frac{\hat{\sigma}_{ij}-\varsigma_{ij}}{\|\hat{\sigma}_{ij}-\varsigma_{ij}\|}+\eta^{K}_{ij}\left(\dot{\beta}^{+}+\dot{\beta}^{-}+\dot{\beta}^{A}\right)\\ &= \frac{2}{3}H\dot{\varepsilon}^{p}_{ij}+\eta^{K}_{ij}\left(\dot{\beta}^{+}+\dot{\beta}^{-}+\dot{\beta}^{A}\right)\end{aligned} \tag{39}$$

$$\begin{aligned}&\dot{\varepsilon}^{trip}_{ij} \in \partial_{R_{ij}}\bar{\Phi}^{m}\\ &= 2\sigma_{ij}\left\{\left(M_{13}\beta^{+}+M_{31}\beta^{A}\right)\dot{\beta}^{+}+\left(M_{32}\beta^{-}+M_{23}\beta^{A}\right)\dot{\beta}^{-}+\right.\\ &\left.+\left[M_{43}\beta^{A}+M_{34}\left(1-\beta^{+}-\beta^{-}-\beta^{A}\right)\right]\dot{\beta}^{A}\right\}\end{aligned} \tag{40}$$

$$\dot{\xi}^{+} \in \partial_{S^{+}}\bar{\Phi}^{m} = \left|\dot{\beta}^{+}\right| \tag{41}$$

$$\dot{\xi}^{-} \in \partial_{S^{-}}\bar{\Phi}^{m} = \left|\dot{\beta}^{-}\right| \tag{42}$$

$$\dot{\xi}^{A} \in \partial_{S^{A}}\bar{\Phi}^{m} = \left|\dot{\beta}^{A}\right| \tag{43}$$

where $M_{13} = M_{31}, M_{23} = M_{32}$ and $M_{34} = M_{43}$, are parameters associated with the TRIP effect; $\eta^{m}(m = +, -, A)$ is associated with the internal dissipation of each material phase, while η^{I} defines the coupling between phase transformations and isotropic

hardening. The coupling with the kinematic hardening is defined by the second-order tensor η_{ij}^{K}.

Besides, $\kappa_{\bar{\chi}} = \kappa_{\bar{\chi}}\left(\mathrm{B}^{+}, \mathrm{B}^{-}, \mathrm{B}^{\mathrm{A}}\right)$ is related to the sub-differential of the indicator function of the convex set $\bar{\chi}$, $\mathrm{I}_{\bar{\chi}}$, with respect to $\mathrm{B}^{+}, \mathrm{B}^{-}$and B^{A}, which defines restrictions associated with phase transformations.

$$\kappa_{\bar{\chi}} = \left(\kappa_{\bar{\chi}}^{+}, \kappa_{\bar{\chi}}^{-}, \kappa_{\bar{\chi}}^{A}\right) \in \partial I_{\bar{\chi}}\left(B^{+}, B^{-}, B^{A}\right) \tag{44}$$

Alternatively, κ_{χ} may be defined as the sub-differential of the indicator function of the convex set χ, I_{χ}, with respect to $\dot{\beta}^{+}, \dot{\beta}^{-}$and $\dot{\beta}^{\mathrm{A}}$.

$$\kappa_{\chi} = \left(\kappa_{\chi}^{+}, \kappa_{\chi}^{-}, \kappa_{\chi}^{A}\right) \in \partial I_{\chi}\left(\dot{\beta}^{+}, \dot{\beta}^{-}, \dot{\beta}^{A}\right) \tag{45}$$

Physically, these restrictions establish conditions for internal sub-loops due to incomplete phase transformations and also avoid improper phase transformations [30]. The definition of this convex set requires an equivalent stress field, similar to the strain field provided in Eq. (1), given by:

$$\Gamma^{\sigma} = \frac{1}{3}\sigma_{kk} + \frac{2}{3}\sqrt{3J_2^{\sigma}}\,\mathrm{sign}(\sigma_{kk}) \tag{46}$$

Besides, it is important to define the quantities at the initial state:

$$\varepsilon_{ij}^{e}(0) = \varepsilon_{ij}^{e} - \frac{\Omega_{ij}(T - T_0)}{E_{ijkl}} \tag{47}$$

$$\Gamma_0 = \frac{1}{3}\varepsilon_{kk}^{e}(0) + \frac{2}{3}\sqrt{3J_2^{e}(0)}\,\mathrm{sign}\left(\varepsilon_{kk}^{e}(0)\right) \tag{48}$$

Now, the convex set χ is defined by considering two different situations associated with mechanical and thermal loadings. Basically, when mechanical loadings govern phase transformations, $\dot{\Gamma}^{\sigma} \neq 0$, the convex set is given by:

$$\chi = \left\{ \dot{\beta}^{n} \in \Re \,\middle|\, \begin{array}{ll} \dot{\Gamma}\dot{\beta}^{+} \geq 0; \dot{\Gamma}\dot{\beta}^{A} \leq 0 & \text{if } \Gamma_0 > 0 \\ \dot{\Gamma}\dot{\beta}^{-} \leq 0; \dot{\Gamma}\dot{\beta}^{A} \geq 0 & \text{if } \Gamma_0 < 0 \end{array} \right\} \tag{49}$$

On the other hand, when thermal loadings govern phase transformation, $\dot{\Gamma}^{\sigma} = 0$, the convex set χ is defined as follows, by considering three subsets (χ_1, χ_2, χ_3):

$$\chi_1 = \left\{ \dot{\beta}^{n} \in \Re \,\middle|\, \dot{T}\dot{\beta}^{A} \geq 0 \right\} \tag{50a}$$

$$\chi_2 = \left\{ \dot{\beta}^{n} \in \Re \,\middle|\, \dot{T}\dot{\beta}^{+} = 0 \begin{bmatrix} \text{if } \dot{T} > 0, \dot{\beta}^{+} > 0 \text{ and } \beta_s^{+} \neq 0 \\ \text{if } \dot{T} > 0, \beta^{+} \neq \beta_s^{+} \text{ and } \beta_s^{+} = 0 \\ \text{if } \dot{T} > 0, \dot{\beta}^{A} = 0 \\ \text{if } \dot{T} < 0, \Gamma^{\sigma} = 0 \text{ and } \beta^{+} \neq \beta_s^{+} \end{bmatrix} \right\} \tag{50b}$$

$$\chi_3 = \left\{ \dot{\beta}^{n} \in \Re \,\middle|\, \dot{T}\dot{\beta}^{-} = 0 \begin{bmatrix} \text{if } \dot{T} > 0, \dot{\beta}^{-} > 0 \text{ and } \beta_s^{-} \neq 0 \\ \text{if } \dot{T} > 0, \beta^{-} \neq \beta_s^{-} \text{ and } \beta_s^{-} = 0 \\ \text{if } \dot{T} > 0, \dot{\beta}^{A} = 0 \\ \text{if } \dot{T} < 0 \, \Gamma^{\sigma} = 0 \text{ and } \beta^{-} \neq \beta_s^{-} \end{bmatrix} \right\} \tag{50c}$$

where β_s^{+} and β_s^{-} are the values of β^{+} and β^{-}, respectively, when the phase transformation begins to take place. Note that this set also expresses restrictions related to improper phase transformations, $M^{+} \rightarrow M$ and $M^{-} \rightarrow M$, expressed respectively, by:

$$\begin{aligned} \dot{\beta}^{+}\dot{\beta}^{M} &= \dot{\beta}^{+}\left(-\dot{\beta}^{+} - \dot{\beta}^{-} - \dot{\beta}^{A}\right) = -\left(\dot{\beta}^{+}\right)^{2} - \dot{\beta}^{+}\dot{\beta}^{A} = 0 \\ \dot{\beta}^{-}\dot{\beta}^{M} &= \dot{\beta}^{-}\left(-\dot{\beta}^{+} - \dot{\beta}^{-} - \dot{\beta}^{A}\right) = -\left(\dot{\beta}^{-}\right)^{2} - \dot{\beta}^{-}\dot{\beta}^{A} = 0 \end{aligned} \tag{51}$$

The definition of the set governed by thermal loadings ($\dot{\Gamma}^{\sigma} = 0$) defines a phase transformation critical stress for twinned martensite, Γ^{C}.

Plastic behavior considers that I_f is the indicator function related to the classical plasticity, being associated with a yield surface defined by f as follows [31].

$$f = \|\hat{\sigma}_{ij} - \varsigma_{ij}\| - \sqrt{\frac{2}{3}}(\sigma_Y - K\vartheta) \tag{52}$$

where the deviatoric tensor, $\hat{\sigma}_{ij}$, is given by:

$$\hat{\sigma}_{ij} = \sigma_{ij} - \frac{1}{3}\sigma_{kk}\delta_{ij} \tag{53}$$

and $\|\hat{\sigma}_{ij} - \varsigma_{ij}\|$ is the euclidean norm of $\hat{\sigma}_{ij} - \varsigma_{ij}$, defined as follows,

$$\|\hat{\sigma}_{ij} - \varsigma_{ij}\| = \sqrt{\sum_{i,j=1}^{3}\left(\hat{\sigma}_{ij} - \varsigma_{ij}\right)^{2}} \tag{54}$$

Plastic behavior is subjected to the Kuhn–Tucker and consistency conditions,

$$\gamma \geq 0, \quad f \leq 0, \quad \gamma f = 0 \quad \text{and} \quad \gamma\dot{f} = 0 \text{ if } f = 0 \tag{55}$$

where γ is the plastic multiplier.

Box 1 Constitutive equations

$$\sigma_{ij} = E_{ijkl}\varepsilon^e_{kl} + \alpha\omega_{ij}\left(\beta^- - \beta^+\right) - \Omega_{ij}(T - T_0)$$

$$\dot{\beta}^+ = \frac{1}{\eta^+}\left\{\Gamma\alpha + \Lambda + P^+ - \alpha^h_{ijkl}r_{kl}\Omega_{ij}(T - T_0) - \eta^I K\vartheta - \eta^K_{ij}\frac{\varsigma_{ij}}{H} - \kappa^+_\pi\right\} + \kappa^+_\chi$$

$$\dot{\beta}^- = \frac{1}{\eta^-}\left\{-\Gamma\alpha + \Lambda + P^- + \alpha^h_{ijkl}r_{kl}\Omega_{ij}(T - T_0) - \eta^I K\vartheta - \eta^K_{ij}\frac{\varsigma_{ij}}{H} - \kappa^-_\pi\right\} + \kappa^-_\chi$$

$$\dot{\beta}^A = \frac{1}{\eta^A}\left\{P^A + \Lambda^{\aleph} + \varepsilon^e_{ij}\left(\Omega^A_{ij} - \Omega^M_{ij}\right)(T - T_0) - \frac{1}{2}\left(K^A - K^M\right)\vartheta^2 - \left(\frac{1}{2H^A} - \frac{1}{2H^M}\right)\varsigma_{ij}\varsigma_{ij} + \eta^I K\vartheta + \eta^K_{ij}\frac{\varsigma_{ij}}{H} - \kappa^A_\pi\right\} + \kappa^A_\chi$$

$$\dot{\varepsilon}^p_{ij} = \gamma\frac{\hat{\sigma}_{ij} - \varsigma_{ij}}{\bar{\sigma}_{ij} - \varsigma_{ij}}\vartheta\dot{} = \sqrt{\tfrac{2}{3}}\gamma + \eta^I\left(\dot{\beta}^+ + \dot{\beta}^- + \dot{\beta}^A\right)$$

$$\dot{\varsigma}_{ij} = \tfrac{2}{3}H\dot{\varepsilon}^p_{ij} + \eta^K_{ij}\left(\dot{\beta}^+ + \dot{\beta}^- + \dot{\beta}^A\right)$$

$$\dot{\varepsilon}^{trip}_{ij} = 2\sigma_{ij}\left\{\left(M_{13}\beta^+ + M_{31}\beta^A\right)\dot{\beta}^+ + \left(M_{32}\beta^- + M_{23}\beta^A\right)\dot{\beta}^- + \left[M_{43}\beta^A + M_{34}\left(1 - \beta^+ - \beta^- - \beta^A\right)\right]\dot{\beta}^A\right\}$$

$$\dot{\xi}^+ = \left|\dot{\beta}^+\right|\dot{\xi}^- = \left|\dot{\beta}^-\right|\dot{\xi}^A = \left|\dot{\beta}^A\right|$$

Yield surface and its conditions:

$$f = \hat{\sigma}_{ij} - \varsigma_{ij} - \sqrt{\tfrac{2}{3}}(\sigma_Y - K\vartheta)$$

$$\gamma \geq 0; f \leq 0 \text{and} \gamma f = 0; \gamma\dot{f} = 0 \text{if } f = 0$$

2.3 Constitutive equations

A complete set of constitutive equations that describes the SMA thermomechanical behavior is now defined being summarized in Box 1.

Model parameters are related to different physical processes, including thermo-elasto-plasticity and phase transformation parameters. In this regard, several parameters are classical from thermo-elasto-plastic theory. TRIP phenomenon is related to some specific parameters, $M_{13} = M_{31}$, $M_{23} = M_{32}$ and $M_{34} = M_{43}$; and also to the modification of nominal values treated in the next section.

The coupling between phase transformation and kinematic hardening is defined by the second-order tensor η^K_{ij} defined as follows:

$$\eta^K_{ij} = \eta^K\begin{bmatrix}1 & 1 & 1\\ 1 & 1 & 1\\ 1 & 1 & 1\end{bmatrix} \tag{56}$$

The definition of the phase transformation critical stress for twinned martensite, Γ^C, can be obtained from the constitutive equations under the following assumptions: $\dot{\beta}^+ = 0, \beta^+ = 0, \beta^- = 0, \beta^A = 0$ and $\Gamma_0 \geq 0$. Therefore, using volume fraction equations, it is possible to write an expression for the critical strain that induces phase transformation from twinned to detwinned martensite:

$$\Gamma^C = \frac{1}{\alpha}\left(-\Lambda - E^M_{ijkl}\varepsilon^e_{kl}\alpha^h_{ijmp}r_{mp} + \alpha^h_{ijkl}r_{kl}\Omega_{ij}(T - T_0) + \eta^I K\vartheta + \eta^K_{ij}\frac{\varsigma_{ij}}{H}\right) \tag{57}$$

Due to tension–compression symmetry, analogous result can be obtained analyzing the evolution equation of β^-.

It is important to highlight that some parameters are split due to temperature or loading dependence. In this regard, some changes can be used to facilitate adjustments with experimental data. For instance, yield surface can be defined as a function of temperature. The same is performed for phase transformation stress levels that are defined as a function of temperature. The dissipation aspects of phase transformation may be defined using different parameters during loading and unloading. In this regard, details of some parameters are presented in the sequence.

Initially, consider the temperature dependent functions $\Lambda = \Lambda(T)$ and $\Lambda^{\aleph} = \Lambda^{\aleph}(T)$. The following definitions are adopted:

$$\Lambda = 2\Lambda^M = \begin{cases} -L^{\pm}_0 + \dfrac{L^{\pm}}{T^M}\left(T - T^M\right) & \text{if } T > T^M \\ -L^{\pm}_0 & \text{if } T \leq T^M \end{cases} \tag{58}$$

$$\Lambda^{\aleph} = \Lambda^M + \Lambda^A = \begin{cases} -L^A_0 + \dfrac{L^A}{T^M}\left(T - T^M\right) & \text{if } T > T^M \\ -L^A_0 & \text{if } T \leq T^M \end{cases} \tag{59}$$

where T^M is the temperature below which the martensitic phase becomes stable for a stress free state; note that the phase transformation stress level is constant for $T < T^M$.

The phase transformation dissipation can be defined taking into account different characteristics of the phase transformation kinetics during loading

and unloading processes. Therefore, different values can be employed for the parameters η^+, η^- and η^A, in the follow form:

$$\begin{cases} \eta^{\pm} = \eta_L^{\pm} & \text{if } \dot{\Gamma} > 0 \\ \eta^{\pm} = \eta_U^{\pm} & \text{if } \dot{\Gamma} < 0 \end{cases} \tag{60}$$

$$\begin{cases} \eta^{A} = \eta_L^{A} & \text{if } \dot{\Gamma} > 0 \\ \eta^{A} = \eta_U^{A} & \text{if } \dot{\Gamma} < 0 \end{cases} \tag{61}$$

where the parameters $\eta_L^{\pm}$, $\eta_U^{\pm}$, η_L^A and η_U^A are calculated considering fourth-order tensors, in the same way of the Eqs. (62) and (63).

$$\begin{cases} (\,) = r_{ij}(\widehat{\ })_{ijkl} r_{kl} & \text{if } \Gamma^{\sigma} \neq 0 \\ (\,) = (\,)_N & \text{otherwise} \end{cases} \tag{62}$$

where

$$(\widehat{\ })_{ijkl} = \begin{bmatrix} (\,)_N & (\,)_N - (\,)_S & (\,)_N - (\,)_S & 0 & 0 & 0 \\ (\,)_N - (\,)_S & (\,)_N & (\,)_N - (\,)_S & 0 & 0 & 0 \\ (\,)_N - (\,)_S & (\,)_N - (\,)_S & (\,)_N & 0 & 0 & 0 \\ 0 & 0 & 0 & 2(\,)_S & 0 & 0 \\ 0 & 0 & 0 & 0 & 2(\,)_S & 0 \\ 0 & 0 & 0 & 0 & 0 & 2(\,)_S \end{bmatrix} \tag{63}$$

where $(\,)_N$ and $(\,)_S$ respectively represents the normal and the shear components.

Concerning plastic effects, the yield surface is defined by the yield stress, σ_Y, that has different values for the austenitic and martensitic phases. Their values are also temperature dependent tending to decrease for high temperatures. Different expressions can be employed for the proper description of these conditions. Here, for the sake of simplicity, temperature variation is assumed to be:

$$\begin{cases} \sigma_Y = \sigma_Y^M & \text{if } T \leq T^M \\ \sigma_Y = \dfrac{\sigma_Y^M (T^A - T) + \sigma_Y^{Ai} (T - T^M)}{T^A - T^M} & \text{if } T^M < T \leq T^A \\ \sigma_Y = \dfrac{\sigma_Y^{Ai} (T^F - T) + \sigma_Y^{Af} (T - T^A)}{T^F - T^A} & \text{if } T^M < T \leq T^F \end{cases} \tag{64}$$

where T^A is the temperature above which the austenitic phase is stable; T^F is a reference temperature for the determination of the yield stress for high temperatures; σ_Y^{Ai} and σ_Y^{Af} define the thermal variation of the yield stress of the austenitic phase.

Figure 1 shows a sketch of inelastic surfaces as a function of temperature. Either phase transformation or yield surfaces are temperature dependent. Phase transformation inelastic surfaces are defined from evolution equations and therefore, they are not straight lines and can vary depending on temperature and strain level. This characteristic makes the model flexible in the sense that it allows the description of several SMA thermomechanical behaviors, using the same set of parameters. The model parameters can be adjusted from tension or torsion tests at different temperatures and define the inelastic surfaces and their evolution with temperature and strain.

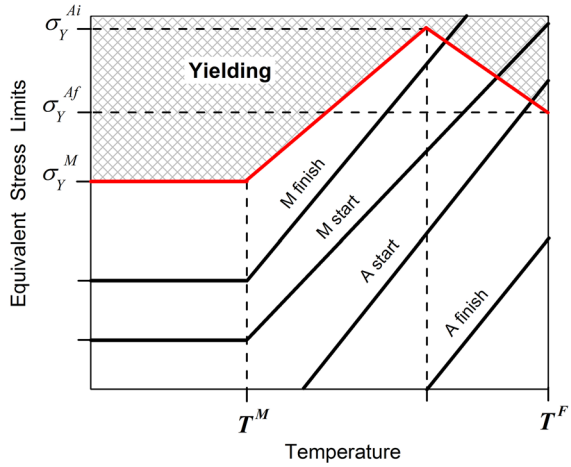

Fig. 1 Inelastic surface sketch

2.3.1 TRIP parameters

TRIP effect influences nominal parameters, defining a saturation effect. This behavior is taken into account with exponential functions, associated the variables ξ^n related TRIP effect. A discussion of these parameters is presented in the sequence.

Parameters α, L_o^+, L_o^-, L_o^A, L^+, L^-, L^A are presented in the general form:

$$\begin{cases} (\,) = (\widehat{\ }) \left[\dfrac{N + \exp\left(-m^{(\,)} \xi^+\right)}{N+1} \right] & \text{if } \Gamma \geq 0 \\ (\,) = (\widehat{\ }) \left[\dfrac{N + \exp\left(-m^{(\,)} \xi^-\right)}{N+1} \right] & \text{if } \Gamma < 0 \end{cases} \tag{65}$$

where $(\,)$ represents the actual value of the parameter, $(\widehat{\ })$ represents the nominal value, $m^{(\,)}$ and N are parameters related to the saturation effect.

In this regard, the vertical size of hysteresis in the stress–strain curve is done through the set parameter α as follows.

$$\begin{cases} \alpha = \hat{\alpha}\left[\dfrac{N+\exp\left(-m^{\alpha}\xi^{+}\right)}{N+1}\right] & \text{if } \Gamma \geq 0 \\ \alpha = \hat{\alpha}\left[\dfrac{N+\exp(-m^{\alpha}\xi^{-})}{N+1}\right] & \text{if } \Gamma < 0 \end{cases} \tag{66}$$

where m^{α} is the parameter related to the saturation effect in order to control α. Similar considerations are adopted for the other parameters.

In addition, the following TRIP parameters are defined:

$$M_{13} = \hat{M}_{13}\exp\left(-m^{M}\xi^{+}\right) \quad M_{31} = \hat{M}_{31}\exp\left(-m^{M}\xi^{+}\right) \tag{67}$$

$$M_{23} = \hat{M}_{23}\exp\left(-m^{M}\xi^{-}\right) \quad M_{32} = \hat{M}_{32}\exp\left(-m^{M}\xi^{-}\right) \tag{68}$$

$$M_{34} = \hat{M}_{34}\exp\left(-m^{M}\xi^{A}\right) \quad M_{43} = \hat{M}_{43}\exp\left(-m^{M}\xi^{A}\right) \tag{69}$$

Table 1 Parameters identified from the experimental results obtained by Tobushi et al. [38] for monotonic pseudoelastic behavior

E^A (GPa)	E^M (GPa)	Ω^A (MPa/K)	Ω^M (MPa/K)	α_N^h (MPa)	$\hat{\alpha}$ (MPa)
54.0	42.0	0.74	0.17	0.0453	330
$\hat{L}_0^{\pm}$ (MPa)	$\hat{L}^{\pm}$ (MPa)	$\hat{L}_0^A$ (MPa)	$\hat{L}^A$ (MPa)	$(\eta_L)_N$ (MPa s)	$(\eta_U)_N$ (MPa s)
0.15	41.50	0.63	180.00	1.00	2.40
$(\eta_L^A)_N$ (MPa s)	$(\eta_U^A)_N$ (MPa s)	T^M (K)	T_0 (K)	σ_Y^M (GPa)	σ_Y^{Ai} (GPa)
1.00	2.40	291.4	307.0	0.5	1.5
σ_Y^{Af} (GPa)	K^A (GPa)	K^M (GPa)	H^A (GPa)	H^M (GPa)	η^I
1.0	1.4	0.4	4.0	1.1	− 0.01
η^K	T^F (K)	$\hat{M}_{13}$ (GPa^{-1})	$\hat{M}_{31}$ (GPa^{-1})	$\hat{M}_{32}$ (GPa^{-1})	$\hat{M}_{23}$ (GPa^{-1})
− 0.01	423.0	0.013	0.010	0.010	0.013
T^{trip} (K)	m^{α}	m^L	m^M	N	
333.0	0.40	0.10	0.50	2	

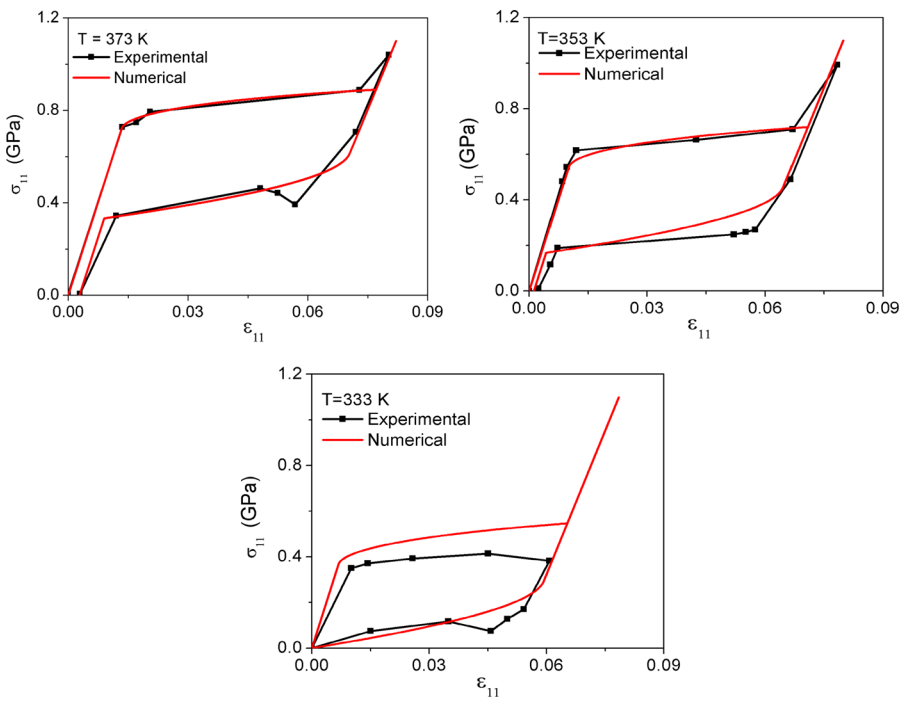

Fig. 2 Pseudoelastic behavior based on experimental data due to Tobushi et al. [38]. Numerical-experimental comparison for $T = 373$ K, $T = 353$ K and $T = 333$

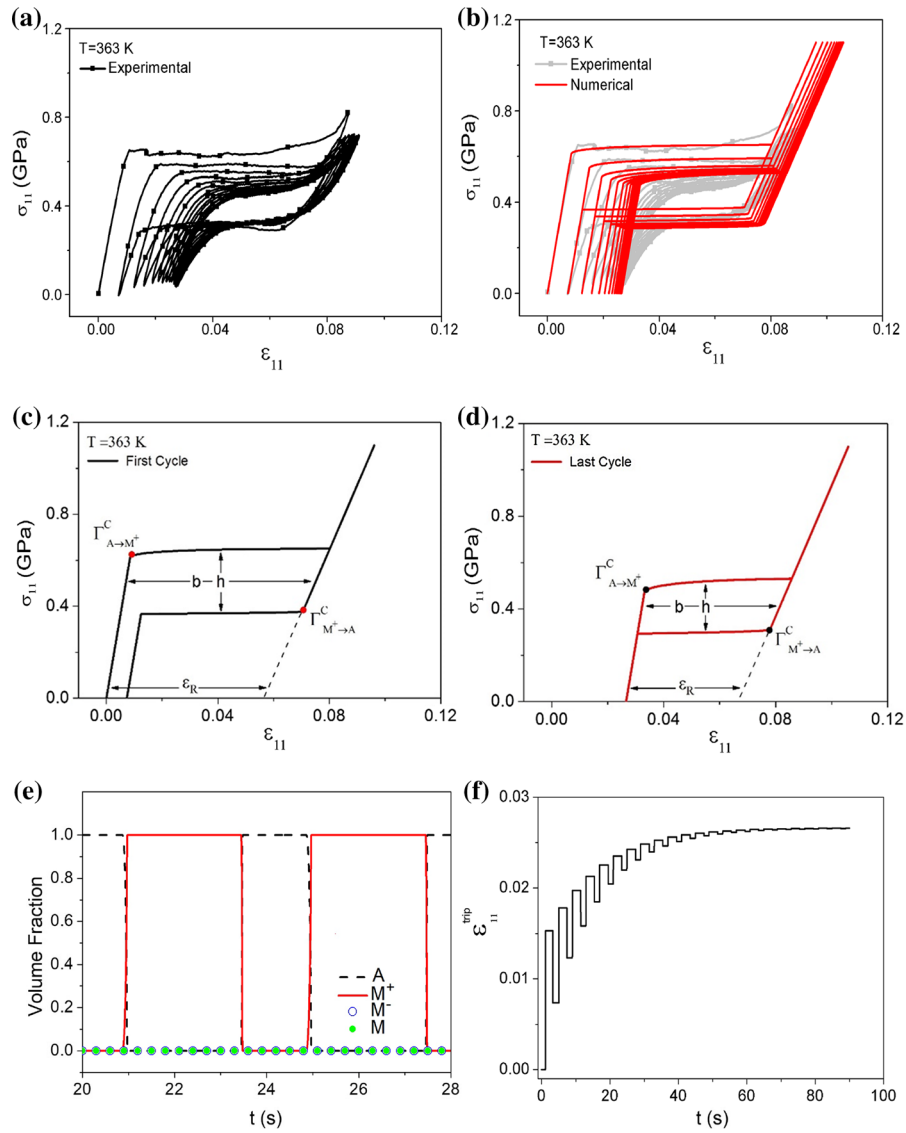

Fig. 3 Pseudoelastic cyclic behavior based on experimental data due to Lagoudas et al. [16]. **a** Experimental stress–strain curve; **b** numerical stress–strain curves; **c** first cycle of the stress–strain curve; **d** last cycle of the stress–strain curve; **e** volume fractions evolution; **f** TRIP strain evolution

where m^M is the parameter related to saturation effect in order to control M_{13}, M_{31}, M_{23}, M_{32}, M_{34} and M_{43}.

In order to control the amount of TRIP strain at different temperatures, the parameters associated with the TRIP effect must also be temperature dependent. By considering a linear dependence, the following expressions are employed:

$$\hat{M}_{13} = \begin{cases} 0 & \text{if } T < T^{trip} \\ \hat{M}^R_{13} \dfrac{(T - T^{trip})}{(T^F - T^{trip})} & \text{if } T \geq T^{trip} \end{cases} \tag{70}$$

where $\hat{M}^R_{13}$ is a reference value of $\hat{M}_{13}$ at $T = T^{trip}$ and T^{trip} is a temperature below which TRIP should not exist. Analogous expressions are used to M_{31}, M_{23} and M_{32}. For the sake of simplicity, this work considers $M_{34} = M_{43} = 0$.

3 Uniaxial tests

The model capability to describe SMA thermomechanical behavior including TRIP is now in focus. Initially, uniaxial tests are treated by assuming that mechanical loading varies linearly from zero to a maximum value and then back to zero without reaching the yield surface. Stress driving case is

Table 2 Parameters identified from experimental results obtained by Lagoudas et al. [16] for pseudoelastic cyclic behavior

E^A (GPa)	E^M (GPa)	Ω^A (MPa/K)	Ω^M (MPa/K)	α_N^h (MPa)	$\hat{\alpha}$ (MPa)
72.0	28.2	0.74	0.17	0.0370	140
$\hat{L}_0^{\pm}$ (MPa)	$\hat{L}^{\pm}$ (MPa)	$\hat{L}_0^A$ (MPa)	$\hat{L}^A$ (MPa)	$(\eta_L)_N$ (MPa s)	$(\eta_U)_N$ (MPa s)
0.10	41.50	0.63	147.00	0.10	0.04
$(\eta_L^A)_N$ (MPa s)	$(\eta_U^A)_N$ (MPa s)	T^M (K)	T_0 (K)	σ_Y^M (GPa)	σ_Y^{Ai} (GPa)
0.10	0.04	291.4	307.0	0.5	1.5
σ_Y^{Af} (GPa)	K^A (GPa)	K^M (GPa)	H^A (GPa)	H^M (GPa)	η^I
1.0	1.4	0.4	4.0	1.1	− 0.01
η^K	T^F (K)	$\hat{M}_{13}$ (GPa^{-1})	$\hat{M}_{31}$ (GPa^{-1})	$\hat{M}_{32}$ (GPa^{-1})	$\hat{M}_{23}$ (GPa^{-1})
− 0.01	423.0	0.072	0.071	0.072	0.071
T^{trip}(K)	m^{α}	m^L	m^M	N	
330.0	0.07	0.20	0.14	2	

Table 3 Characteristic of the first and last stress–strain loops

	First cycle	Last cycle	Variation (%)
$\Gamma^C_{A\to M^+}$ (GPa)	0.62	0.48	− 22.6
$\Gamma^C_{M^+\to A}$ (GPa)	0.38	0.31	− 18.4
h (GPa)	0.28	0.22	− 21.4
b	0.07	0.05	− 28.6
ε_R	0.06	0.04	− 33.3

assumed. Table 1 presents constitutive parameters identified from experimental results due to Tobushi et al. [38] that consider pseudoelastic behavior for different temperatures. In order to compare with the one-dimensional model, Poisson's ratio is vanished.

Figure 2 presents the comparison between numerical simulations provided by the proposed model with experimental data from Tobushi et al. [38] for three different temperatures: T = 373 K, T = 353 K and T = 333 K. It is noticeable that the model captures the general thermomechanical behavior, especially the TRIP effect. Note that when the loading cycle is finished, the system presents a residual strain, and yield surface is not reached. This behavior is temperature dependent and the effect decreases with temperature decrease. It should be highlighted that the TRIP effect does not occur for low temperature, related to the martensitic phase.

TRIP effect has a saturation characteristic meaning that its manifestation reduces when the number of cycles increases. Because of that, SMA is usually subjected to a training process that stabilizes the SMA response. Basically, the training process imposes a

Table 4 Parameters identified from experimental results obtained by Garcia [11] for pseudoelastic cyclic behavior involving classical plasticity

E^A (GPa)	E^M (GPa)	Ω^A (MPa/K)	Ω^M (MPa/K)	α_N^h (MPa)	$\hat{\alpha}$ (MPa)
62.0	25.0	0.74	0.17	0.0120	200
$\hat{L}_0^{\pm}$ (MPa)	$\hat{L}^{\pm}$ (MPa)	$\hat{L}_0^A$ (MPa)	$\hat{L}^A$ (MPa)	$(\eta_L)_N$ (MPa s)	$(\eta_U)_N$ (MPa s)
4.00	3.00	0.03	52.00	0.60	0.50
$(\eta_L^A)_N$ (MPa s)	$(\eta_U^A)_N$ (MPa s)	T^M (K)	T_0 (K)	σ_Y^M (GPa)	σ_Y^{Ai} (GPa)
0.60	0.50	282.1	303.0	0.5	1.5
σ_Y^{Af} (GPa)	K^A (GPa)	K^M (GPa)	H^A (GPa)	H^M (GPa)	η^I
1.0	1.4	0.4	4.0	1.1	− 0.01
η^K	T^F (K)	$\hat{M}_{13}$ (GPa^{-1})	$\hat{M}_{31}$ (GPa^{-1})	$\hat{M}_{32}$ (GPa^{-1})	$\hat{M}_{23}$ (GPa^{-1})
− 0.01	374.0	0.125	0.125	0.125	0.125
T^{trip}(K)	m^{α}	m^L	m^M	N	
310.0	0.0001	0.30	0. 48	0.9	

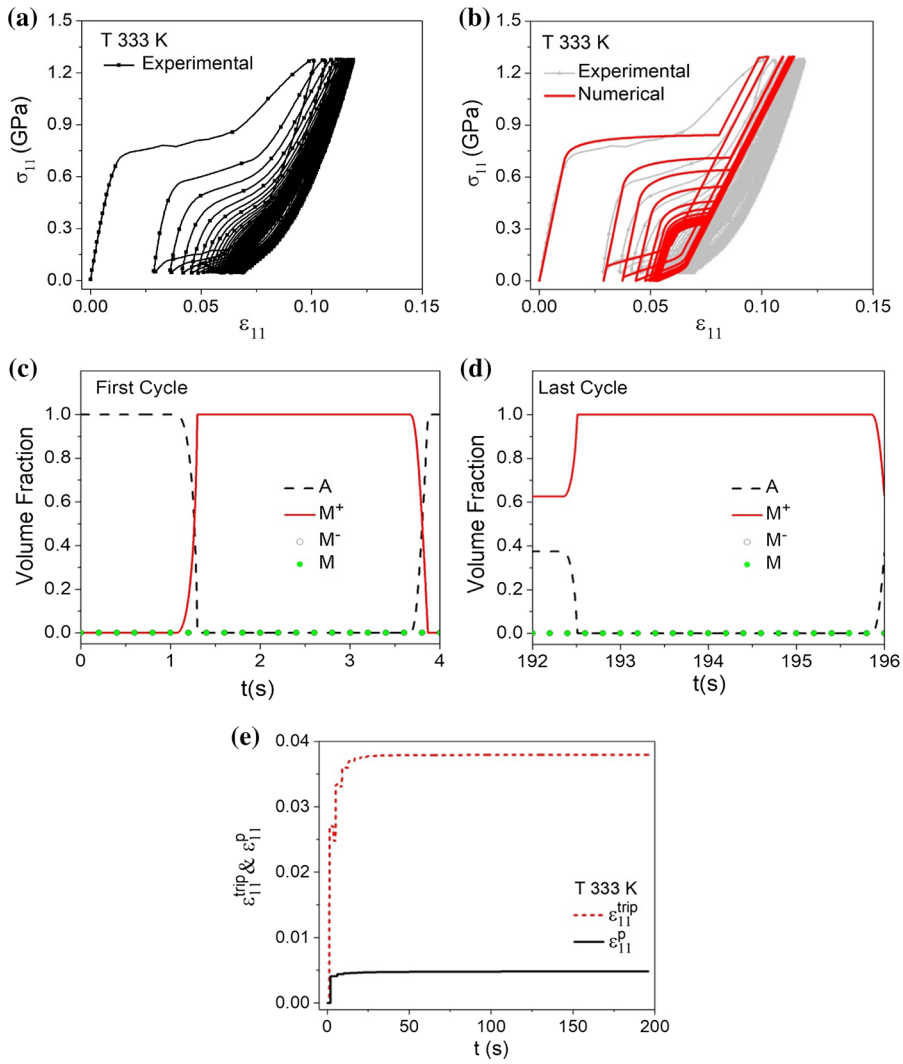

Fig. 4 Pseudoelastic cyclic plastic behavior based on experimental data due to Garcia [11]. **a** Experimental stress–strain curve; **b** numerical stress–strain curves; **c** first cycle of the volume fraction; **d** last cycle of the volume fraction; **e** TRIP strain evolution

Table 5 Parameters identified from experimental results obtained by Sittner et al. [32] for tension–torsion tests

E^A (GPa)	E^M (GPa)	Ω^A (MPa/K)	Ω^M (MPa/K)	α_N^h (MPa)	α_S^h (MPa)
65.0	29.0	0.74	0.17	0.0150	0.0160
$\hat{\alpha}$ (MPa)	$\hat{L}_0^{\pm}$ (MPa)	$\hat{L}^{\pm}$ (MPa)	$\hat{L}_0^A$ (MPa)	$\hat{L}^A$ (MPa)	$(\eta_L)_N$ (MPa s)
140	1.50	5.00	2.00	26.00	5.70
$(\eta_U)_N$ (MPa s)	$(\eta_L^A)_N$ (MPa s)	$(\eta_U^A)_N$ (MPa s)	$(\eta_L)_S$ (MPa s)	$(\eta_U)_S$ (MPa s)	$(\eta_L^A)_S$ (MPa s)
12.00	25.00	3.50	4.85	14.00	10.00
$(\eta_U^A)_S$ (MPa s)	T^M (K)	T_0 (K)	σ_Y^M (GPa)	σ_Y^{Ai} (GPa)	σ_Y^{Af} (GPa)
1.80	223.0	285.0	0.5	1.5	1.0
K^A (GPa)	K^M (GPa)	H^A (GPa)	H^M (GPa)	η^I	η^K
1.4	0.4	4.0	1.1	− 0.01	− 0.01
T^F (K)	$\hat{M}_{13}$ (GPa^{-1})	$\hat{M}_{31}$ (GPa^{-1})	$\hat{M}_{23}$ (GPa^{-1})	$\hat{M}_{32}$ (GPa^{-1})	T^{trip} (K)
423.0	0.072	0.071	0.072	0.071	270.0
m^{α}	m^L	m^M	N	υ^A	υ^M
0.07	0.20	0.14	2	0.36	0.36

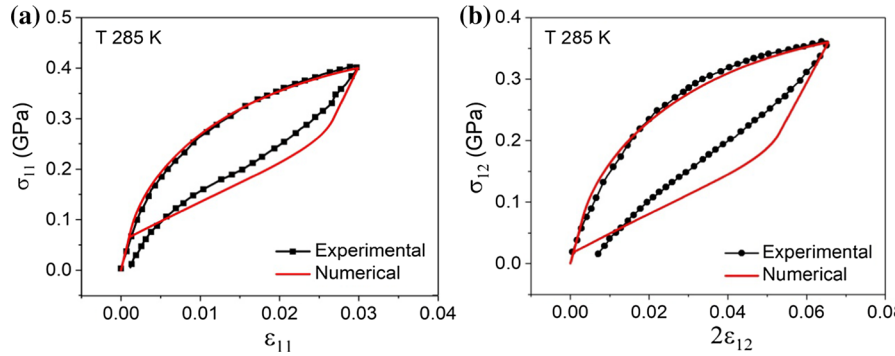

Fig. 5 Uncoupled tension–torsion tests. **a** Tension test; **b** torsion test

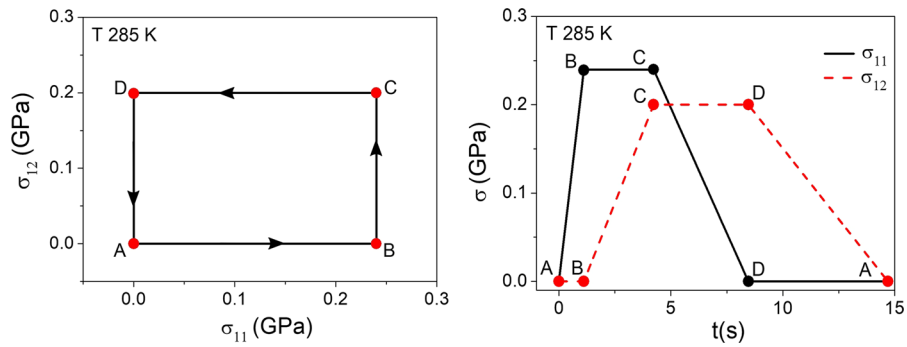

Fig. 6 Loading process of the coupled tension–torsion test

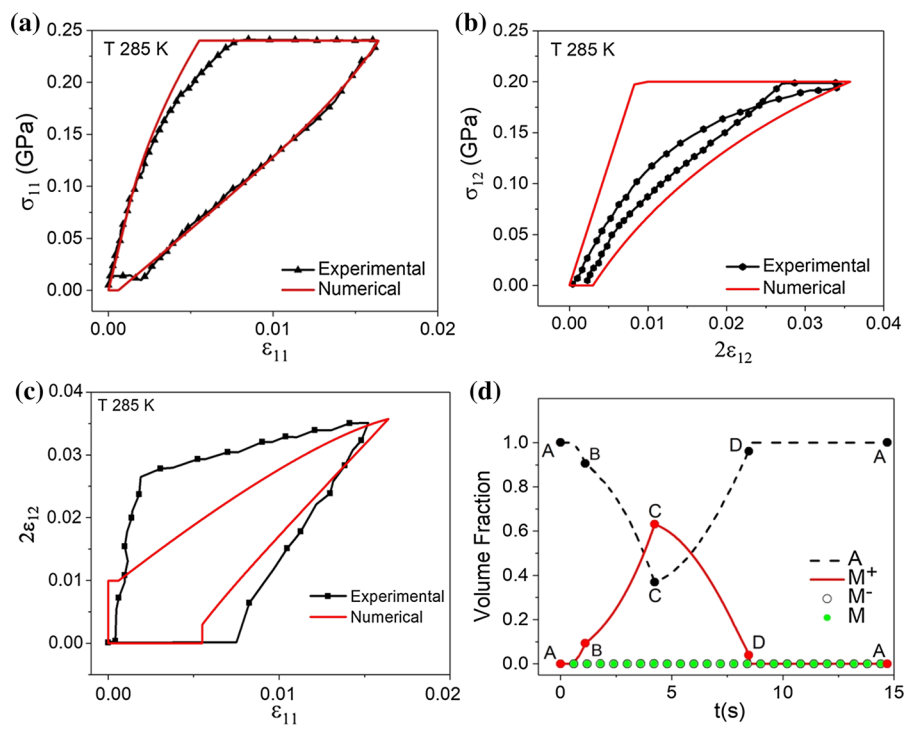

Fig. 7 Coupled tension–torsion test. Stress–strain curves **a** $\sigma_{11} \times \varepsilon_{11}$; **b** $\sigma_{12} \times 2\varepsilon_{12}$; **c** $2\varepsilon_{12} \times \varepsilon_{11}$; **d** volume fractions

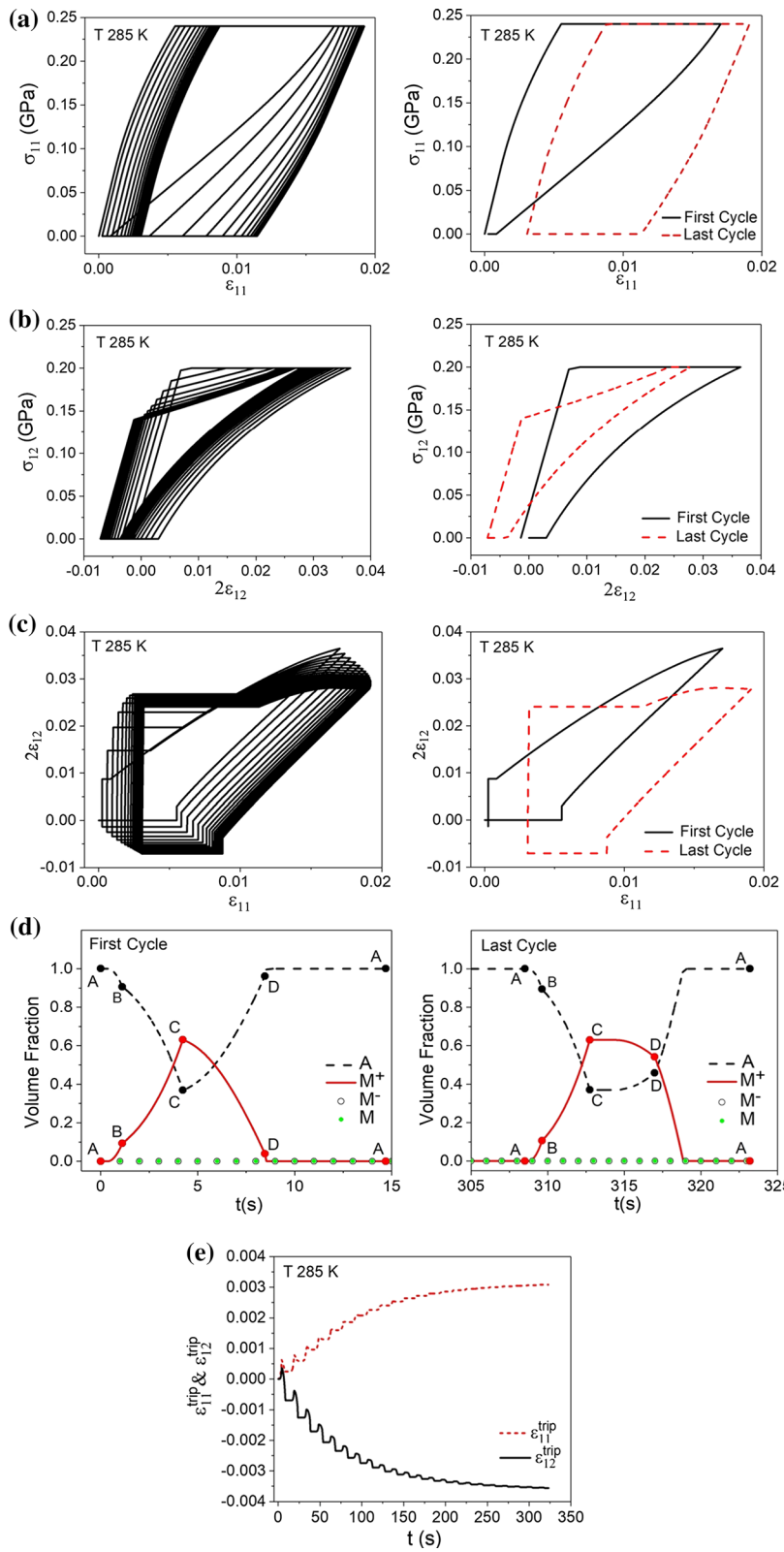

Fig. 8 Coupled tension–torsion cyclic loading test. **a** $\sigma_{11} \times \varepsilon_{11}$; **b** $\sigma_{12} \times 2\varepsilon_{12}$; **c** $2\varepsilon_{12} \times \varepsilon_{11}$; **d** volume fractions; **e** TRIP strains, ε_{11}^{trip} and ε_{12}^{trip}

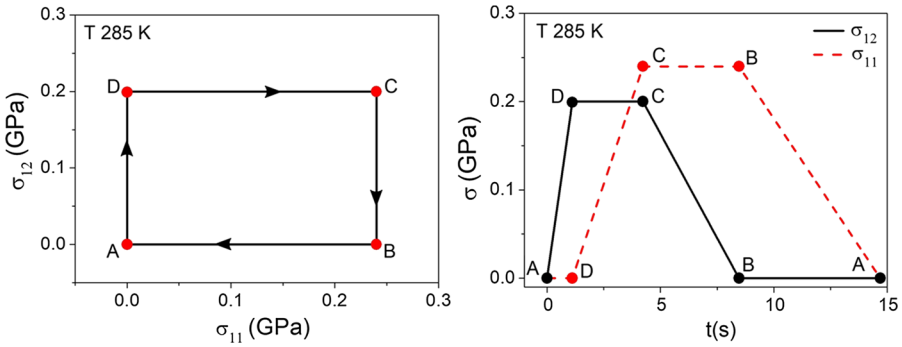

Fig. 9 Loading process of the coupled tension–torsion test

cyclic loading process until the thermomechanical behavior stabilizes. Figure 3 presents experimental data due to Lagoudas et al. [16] used for comparison with numerical simulations. Table 2 presents model parameters identified for simulations. Note that the SMA response presents saturation, stabilizing the stress–strain response after some cycles. Figure 3a shows experimental stress–strain curves while Fig. 3b presents numerical simulations, together with experimental data. It should be pointed out the good agreement between numerical and experimental results, showing the model capability to represent the saturation phenomenon. For each cycle, there is a reduction of the phase transformation critical stress and also a modification of the size of the hysteresis loop. Figure 3c, d present respectively, the stress–strain curve for the first and last cycles allowing one to observe the differences. Note that saturation effect, which occurs around fifteen cycles, is related to a TRIP strain constant value (Fig. 3f), defining a stabilized stress–strain hysteresis loop. Hysteresis loop characteristics show a reduction from 20 to 30%, as can be observed in Table 3 that illustrates the characteristic parameters depicted in Fig. 3c, d. Figure 3e shows the phase transformation evolution during the test presenting the time history of volume fractions for two intermediate cycles. Figure 3f shows the evolution of the TRIP strain. This kind of analysis is interesting in order to evaluate the number of cycles needed for a proper training process.

Classical plasticity is now of concern considering a loading process that reaches the yield surface. Therefore, TRIP effect is treated together with classical plasticity. It is expected that plastic strains inhibit the reverse phase transformation and this effect becomes gradually more pronounced with the increase of plasticity level. Hence, for a low plasticity level, it is expected that reverse transformation takes place. Experimental results due Garcia [11] considering pseudoelastic test together with plasticity are used as reference for numerical simulations. Table 4 presents identified parameters employed on numerical simulations. Figure 4 shows numerical simulations together with experimental data. Figure 4a shows experimental tests due to Garcia [11] while Fig. 4b presents a comparison between numerical and experimental results, showing a good agreement. Figure 4c-d shows volume fraction evolution for the first and last cycles. Figure 4e presents TRIP strain evolution. It is noticeable that plastic behavior, either classical and transformation induced plasticity, tends to alter macroscopic SMA response characteristics. Volume fraction evolutions evidence this conclusion (Fig. 4c, d).

4 Multiaxial tests

A coupled tension–torsion test based on experimental results due to Sittner et al. [32] is now in focus. Initially, model parameters are adjusted by considering uniaxial tension and torsion tests, separately, neglecting TRIP and plasticity. Afterward, the coupled test is carried out using the adjusted parameters defined from the uncoupled tests. Table 5 presents model parameters employed to match uncoupled experimental tests. Other parameters, including classical plasticity and TRIP, are assumed to be the same of the ones obtained on Lagoudas et al. [16] tests (Table 2). Results of the uncoupled tests are presented

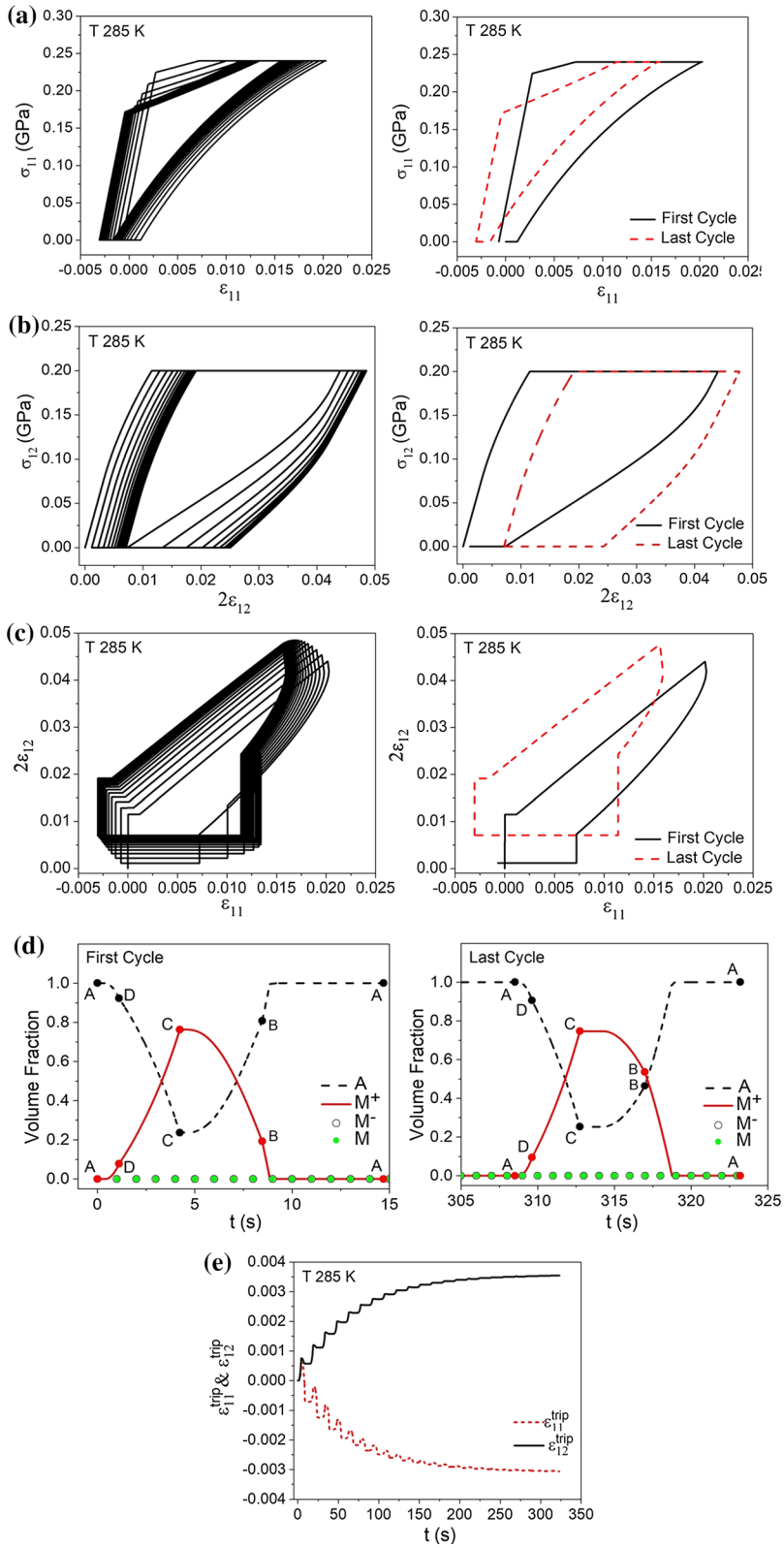

Fig. 10 Coupled tension–torsion cyclic loading test. **a** $\sigma_{11} \times \varepsilon_{11}$; **b** $\sigma_{12} \times 2\varepsilon_{12}$; **c** $2\varepsilon_{12} \times \varepsilon_{11}$; **d** volume fractions; **e** TRIP strains, ε_{11}^{trip} and ε_{12}^{trip}

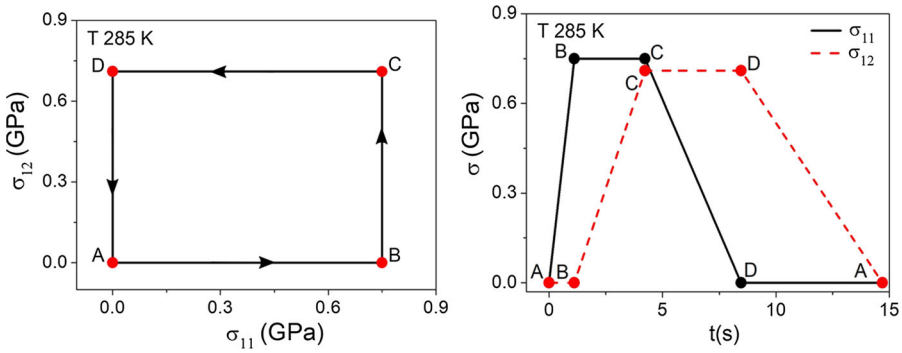

Fig. 11 Loading process of the coupled tension–torsion test with plasticity

in Fig. 5 showing the comparison between numerical results and experimental data due to Sittner et al. [32] for both tension and torsion tests. In these results, TRIP parameters are assumed to vanish. Stress driving simulation is performed.

A coupled tension–torsion test is of concern using the same parameters of the uncoupled test. This test is associated with a square mechanical loading process (ABCD) presented in Fig. 6 and constant temperature ($T = 285$ K). The loading process is composed by a mechanical tensile loading (AB) followed by a mechanical shear loading (BC), which values are not sufficient to reach yield surface. The unloading process starts with a tension unloading (CD) followed by a shear unloading (DA). SMA response is presented in different ways in Fig. 7: stress–strain curves for tension ($\sigma_{11} \times \varepsilon_{11}$), Fig. 7a, and torsion ($\sigma_{12} \times 2\varepsilon_{12}$), Fig. 7b; strain curve $\varepsilon_{11} \times 2\varepsilon_{12}$ (Fig. 7c); volume fraction evolution (Fig. 7d). It is possible to observe that the model captures the general qualitative behavior of the SMA in three-dimensional media with coupled loadings. It is also noticeable that phase transformations occur due normal and shear stresses. It should be highlighted that phase transformation occurs during ABC paths, and most of the volume fraction is formed when both normal and shear stress are applied together (Fig. 7d). The same behavior is observed during unloading.

After model verification for multiaxial test, TRIP behavior is now of concern considering that the SMA sample is subjected to 22 cycles, each of them with the same loading path presented in the previous simulation (Fig. 6). Figure 8 shows the SMA response for the tension–torsion test. The following curves are presented: stress–strain curves for both tension ($\sigma_{11} \times \varepsilon_{11}$) and torsion ($\sigma_{12} \times 2\varepsilon_{12}$); strain curves ($2\varepsilon_{12} \times \varepsilon_{11}$); volume fractions; and TRIP strain evolution (ε_{11}^{trip} and ε_{12}^{trip}). For each one of these curves, results for the first and last cycles are presented, highlighting the difference between them and showing the stabilization process. Volume fractions indicate the phase transformations involved (Fig. 8d). Note that both normal and shear stresses induce phase transformations that are changing between austenite and tensile detwinned martensite. The tension loading (AB) is not sufficient to promote complete phase transformation that is reached after the shear loading (BC). For the unloading process, all the reverse phase transformation occurs in the shear unloading stage during the first cycle. Nevertheless, this changes for the last cycle and reverse phase transformation only finishes after the normal stress unloading. It should be pointed out the difference between phase transformation on the first and last cycles (Fig. 8d).

The SMA specimen is now subjected to a different loading history. Basically, the same coupled tension–torsion test is considered, with the same stress levels, but the square loading path sequence is inverted (Fig. 9). Now, the sequence ADCBA is used instead of ABCDA imposed in the previous simulation. Hence, the loading process is composed by a mechanical torsion loading (AD) followed by a mechanical tensile loading (DC). The unloading process starts with a torsion unloading (CB) followed by a tensile unloading (BA). The SMA sample is subjected to 22 cycles.

Figure 10 presents the SMA response for this tension–torsion test, represented by the following curves: stress–strain curves for both tension ($\sigma_{11} \times \varepsilon_{11}$) and torsion ($\sigma_{12} \times 2\varepsilon_{12}$); strain curves ($2\varepsilon_{12} \times \varepsilon_{11}$); volume fractions; and TRIP strain evolution (ε_{11}^{trip} and ε_{12}^{trip}). For each one of these curves, results for the first and last cycles are presented,

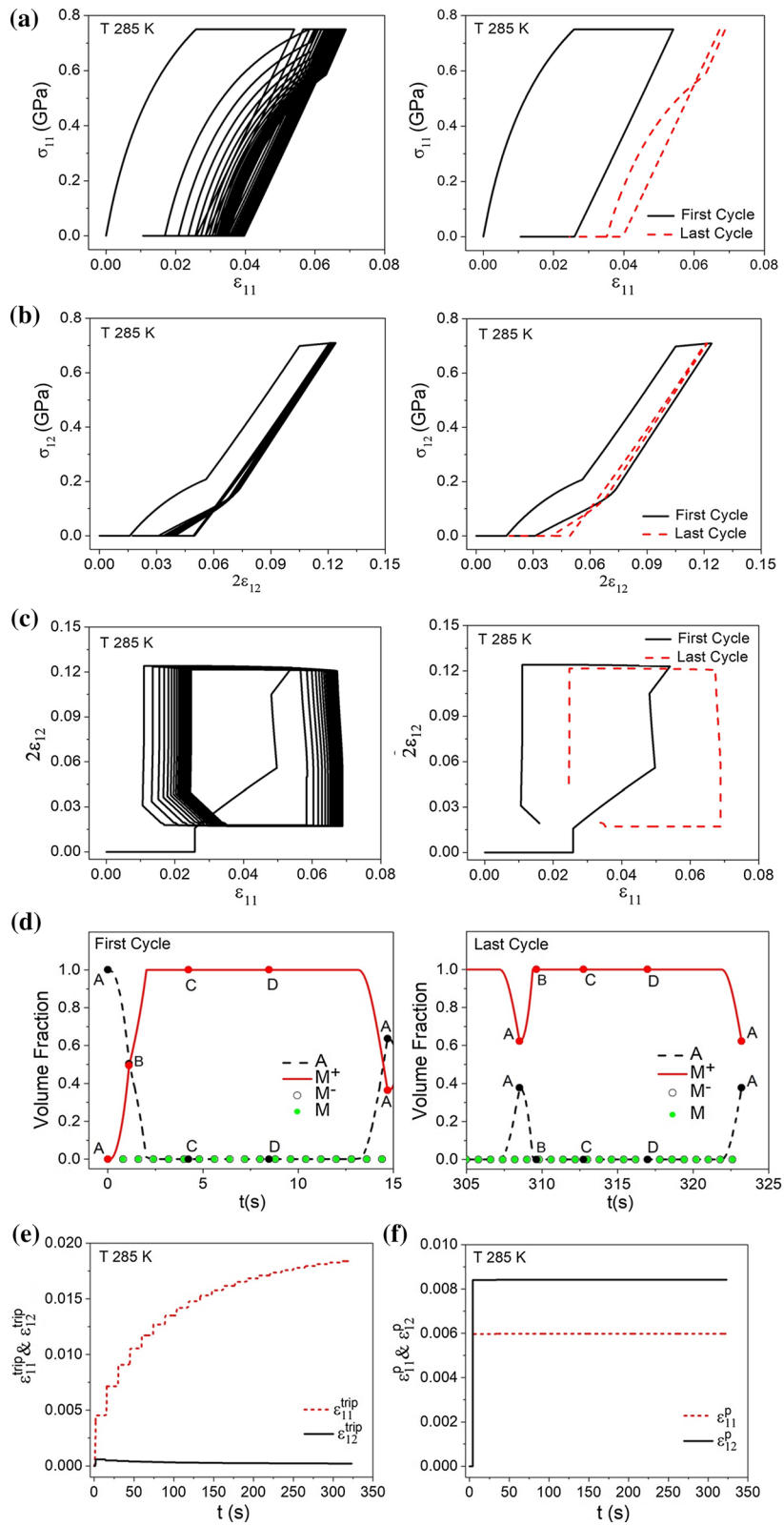

Fig. 12 Coupled tension–torsion cyclic loading test with plasticity. **a** $\sigma_{11} \times \varepsilon_{11}$; **b** $\sigma_{12} \times 2\varepsilon_{12}$; **c** $2\varepsilon_{12} \times \varepsilon_{11}$; **d** volume fractions; **e** TRIP strains, ε_{11}^{trip} and ε_{12}^{trip}; **f** plastic strains, ε_{11}^{p} and ε_{12}^{p}

highlighting the difference between them. In general, it is observed an inversion of the main aspects of the SMA behavior. Results are qualitatively similar to the one presented in Fig. 8, but inverting the tension and torsion strain space.

Multiaxial test with plastic behavior is now in focus, considering a loading history that reaches the yield surface. Figure 11 presents the tension–torsion loading history, assuming the sequence ABCDA. The loading process is initiated by a tension loading (AB), followed by a torsion loading (BC). The unloading is carried out by considering tension unloading (CD), followed by the torsion unloading (DA).

Figure 12 shows the SMA response for the tension–torsion test with plasticity, presenting the following curves that highlight the first and last cycles: stress–strain curves for both tension ($\sigma_{11} \times \varepsilon_{11}$) and torsion ($\sigma_{12} \times 2\varepsilon_{12}$); strain curves ($2\varepsilon_{12} \times \varepsilon_{11}$); volume fractions; TRIP strain evolution (ε_{11}^{trip} and ε_{12}^{trip}); and plastic strain evolution (ε_{11}^{p} and ε_{12}^{p}). It is noticeable that the plastic effect alters significantly the SMA response. It should be pointed out that the last cycle has hysteresis loops smaller than the ones without plastic strains, indicating that plastic strains inhibit phase transformations. This is more evident observing the differences between the first and last cycles of the volume fractions (Fig. 12d). Incomplete reverse phase transformation occurs in the unloading stages of the last cycles. It is also observed that the tension TRIP strain is greater than torsion ones and the opposite occurs in terms of plastic strains (Fig. 12e).

5 Conclusions

This work presents a three-dimensional constitutive model to describe SMA thermomechanical behavior including classical plasticity and transformation induced plasticity. The model is based on the model proposed by Oliveira et al. [24] being extended to consider new state variables associated with TRIP effect. Numerical simulations are compared with experimental data, being in close agreement for both uniaxial and multiaxial tests, presenting proper model verification. General numerical simulations are carried out showing the model capability to describe several phenomena related to SMAs, including classical and transformation induced plasticity. In general, it should be pointed out that, once adjusted, the model is able to reproduce several phenomena in a flexible way, using the same set of parameters. The proposed model presents an interesting tool describe the general SMA thermomechanical behavior, assisting a definition of training processes, identifying the number of cycles necessary for the stabilization and the reduction of critical stresses and hysteresis loop.

Acknowledgements The authors would like to acknowledge the support of the Brazilian Research Agencies CNPq, CAPES and FAPERJ. The Air Force Office of Scientific Research (AFOSR) is also acknowledged.

References

1. Auricchio F, Marfia S, Sacco E (2002) Modeling of SMA materials: training and two way memory effects. Comput Struct 81(24):2301–2317
2. Chemisky Y, Chatzigeorgiou G, Kumar P, Lagoudas DC (2013) A constitutive model for cyclic actuation of high-temperature shape memory alloys. Mech Mater 68:120–136
3. Cherkaoui M, Berveiller M, Sabar H (1998) Micromechanical modeling of martensitic transformation induced plasticity (TRIP) in austenitic single crystals. Int J Plast 14(7):597–626
4. Cissé C, Zaki W, Gu X, Zineb TB (2017) A nonlinear 3D model for iron-based shape memory alloys considering different thermomechanical properties for austenite and martensite and coupling between transformation and plasticity. Mech Mater 107:1–21
5. Coleman BD, Gurtin ME (1967) Thermodynamics with internal state variables. J Chem Phys 47(2):597–613
6. Entchev PB, Lagoudas DC (2004) Modeling of transformation-induced plasticity and its effect on the behavior of porous shape memory alloys. Part II: porous SMA response. Mech Mater 36(9):893–913
7. Fischer FD, Oberaigner ER, Tanaka K, Nishimura F (1998) Transformation induced plasticity revised an update formulation. Int J Solids Struct 35(18):2209–2227
8. Fischer FD, Reisner G, Werner E, Tanaka K, Cailletaud G, Antretter T (2000) A new view on transformation induced plasticity. Int J Plast 16(7):723–748
9. Freed Y, Aboudi J (2009) Thermomechanically coupled micromechanical analysis of shape memory alloy composites undergoing transformation induced plasticity. J Intell Mater Syst Struct 20(1):23–38
10. Ganghoffer JF, Simonsson K (1998) A micromechanical model of the martensitic transformation. Mech Mater 27(3):125–144
11. Garcia MS (2015) Experimental analysis of the thermomechanical behavior of shape memory alloys. Ph.D. Thesis, COPPE/UFRJ—Department of Mechanical Engineering (**in Portuguese**)
12. Gautier E, Zhang XM, Simon A (1989) Role of internal stress state on transformation induced plasticity and transformation mechanisms during the progress of stress induced

phase transformation. In: Beck G, Denis S, Simon A (eds) International conference on residual stresses—ICRS2. Elsevier Applied Science, London, pp 777–783
13. Gautier E (1998) Déformation de transformation et plasticité de transformation. École d'été MH2M, Méthodes d'Homogénéisation en Mécanique des Matériaux, La Londe Les Maures (Var, France)
14. Greenwood GW, Johnson RH (1965) The deformation of metals under small stresses during phase transformation. Proc R Soc 283(1394):403–422
15. Kang G, Kan Q, Qian L, Liu Y (2009) Ratchetting deformation of super-elastic and shape memory NiTi alloys. Mech Mater 41(2):139–153
16. Lagoudas DC, Entchev PB, Kumar PK (2003) Thermomechanical characterization of SMA actuators under cyclic loading. In: Proceedings of IMECE'03, ASME international mechanical engineering congress
17. Lagoudas DC (2008) Shape memory alloys: modeling and engineering applications. Department of Aerospace Engineering Texas A&M University. Springer Science Business Media, LLC, Berlin
18. Lagoudas DC, Entchev PB (2004) Modeling of transformation-induced plasticity and its effect on the behavior of porous shape memory alloys. Part I: constitutive model for fully dense SMAs. Mech Mater 36(9):865–892
19. Leblond J (1989) Mathematical modeling of transformation plasticity in steels II: coupling with strain hardening phenomena. Int J Plast 5(6):573–591
20. Leblond JB, Devaux J, Devaux JC (1989) Mathematical modeling of transformation plasticity in steels I: case of ideal-plastic phases. Int J Plast 5(6):551–572
21. Lemaitre J, Charboche JL (1990) Mechanics of solid materials. Cambridge University Press, Cambridge
22. Magee CL (1966) Transformation kinetics, microplasticity and aging of martensite in Fe–31 Ni. Ph.D. Thesis, Carnegie Institute of Technology, Pittsburg, PA
23. Marketz F, Fischer FD (1994) A micromechanical study on the coupling effect between microplastic deformation and martensitic transformation. Comput Mater Sci 3(2):307–325
24. Oliveira SA, Savi MA, Zouain N (2016) A three-dimensional description of shape memory alloy thermomechanical behavior including plasticity. J Braz Soc Mech Sci Eng 38(5):1451–1472
25. Paiva A, Savi MA (2006) An overview of constitutive models for shape memory alloys. Math Probl Eng 1–30. https://doi.org/10.1155/MPE/2006/56876
26. Paiva A, Savi MA, Braga AMB, Pacheco PMCL (2005) A constitutive model for shape memory alloys considering tensile-compressive asymmetry and plasticity. Int J Solids Struct 42(11-12):3439–3457
27. Paradis A, Terriault P, Brailovski V (2009) Modeling of residual strain accumulation of NiTi shape memory alloys under uniaxial cyclic loading. Comput Mater Sci 47(2):373–383
28. Piecyska E, Gadaj S, Nowacki WK, Hoshio K, Machino Y, Tobushi H (2005) Characteristics of energy storage and dissipation in TiNi shape memory alloys. Sci Technol Adv Mater 6(8):889–894
29. Sakhaei AH, Lim K (2016) Transformation induced plasticity in high temperature shape memory alloys: a one dimensional continuum model. Continuum Mech Thermodyn 28(4):1039–1047
30. Savi MA, Paiva A (2005) Describing internal subloops due to incomplete phase transformations in shape memory alloys. Arch Appl Mech 74(9):637–647
31. Simo JC, Hughes TJR (1998) Computational inelasticity. Springer, Berlin
32. Sittner P, Hara Y, Tokuda M (1995) Experimental study on the thermoelastic martensitic transformation in shape memory alloy polycrystal induced by combined external forces. Metall Mater Trans 26(11):2923–2935
33. Stringfellow RG, Parks DM, Olson GB (1992) A constitutive model for transformation plasticity accompanying strain-induced martensitic transformation in metastable austenitic steels. Acta Metall 40(7):1703–1716
34. Taleb L, Cavallo N, Waeckel F (2001) Experimental analysis of transformation plasticity. Int J Plast 17(1):1–20
35. Taleb L, Sidoroff F (2003) A micromechanical modeling of the Greenwood-Johnson mechanism in transformation induced plasticity. Int J Plast 19(10):1821–1842
36. Tanaka K, Sato Y (1985) A mechanical view of transformation-induced plasticity. Ing Arch 55:147–155
37. Tanaka K, Nishimura F, Hayashi T, Tobushi H, Lexcellent C (1995) Phenomenological analysis on subloops and cyclic behavior in shape memory alloys under mechanical and/or thermal loads. Mech Mater 19(4):281–292
38. Tobushi H, Iwanaga H, Tanaka K, Hori T, Sawada T (1991) Deformation behavior of Ni–Ti shape memory alloy subjected to variable stress and temperature. Continuum Mech Thermodyn 3(2):79–93
39. Yu C, Kang G, Kan Q (2015) A micromechanical constitutive model for anisotropic cyclic deformation of superelastic NiTi shape memory alloy single crystals. J Mech Phys Solids 82:97–136
40. Yu C, Kang G, Kan Q (2014) A physical mechanism based constitutive model for temperature-dependent transformation ratchetting of NiTi shape memory alloy: one-dimensional model. Mech Mater 78:1–10
41. Yu C, Kang G, Kan Q, Song D (2012) A micromechanical constitutive model based on crystal plasticity for thermomechanical cyclic deformation of NiTi shape memory alloys. Int J Plast 44:161–191
42. Zaki W, Mounmi Z (2007) 3D model of the cyclic thermomechanical behavior of shape memory alloys. J Mech Phys Solids 55(11):2427–2454
43. Zhang X, Yan X, Xie H, Sun R (2014) Modeling evolutions of plastic strain, maximum transformation strain and transformation temperatures in SMA under superelastic cycling. Comput Mater Sci 81:113–122
44. Zwigl P, Dunand DC (1997) A nonlinear model for internal stress superelasticity. Acta Mater 45(12):5285–5294